ADDIS ABABA UNIVERSITY

INSTITUTE OF TECHNOLOGYS

SCHOOL OF GRADUATE STUDIES

Thermal Stress Analysis of Disc Brake Rotor By Finite Element Method

A Thesis Submitted to the Graduate School of Addis Ababa University in Partial Fulfillment of the Requirements for the Degree of Masters of Science

In

Mechanical Engineering (Mechanical Design)

By: Kajela Temesgen Deressa

Advisor: Dr. Daniel Tilahun

December, 2013

`

Addis Ababa University

Addis Ababa institute of Technology

School of Mechanical and Industrial Engineering

Thermal Stress Analysis of Disc Brake Rotor by Finite Element Method

By Kajela Temesgen Deressa

Approved by board of Examiners

Daniel Tilahun (Dr.)	_____	_____
Chairman of the school	Signature	Date
Dr. Daniel Tilahun	_____	_____
Advisor	Signature	Date
Dr.-Ing. Zewdu Abdi	_____	_____
Internal Examiner	Signature	Date
Dr.-Ing. Tamrat Tesfaye	_____	_____
External Examiner	Signature	Date

`

Table of Contents

Abstract

Disc brakes are exposed to large temperature resulting large thermal stress during routine braking. These large temperature extrusions have two possible outcomes: fade that generates reduction in stopping power; and large amount of plastic deformation that generates low fatigue life in the brake rotor. The aim of the present work is to investigate the temperature and thermal stress response of gray cast iron disc brake during first braking phase using analytical, as well as finite element (FE) method and comparing the result. The area of study is concentrated on temperature variation as a function of thickness only. Only the areas exposed to high temperature is selected for analysis, specifically the rotor, by excluding hub and vanes because they are for from disc-pad contact. One particular existing brake disc design for a SUV car of model DD6470C is chosen for the investigation. The dimensions, material property and maximum allowable speed of this car are used as an input both for analytical and finite element method. Analytically the distribution of temperature caused by applied heat flux as a function of disc thickness is solved by the method of partial solutions. The finite element simulation for the coupled transient thermal field and stress field is carried out by separate data base thermal-structural coupled method based on ANSYS 14.0 to evaluate the stress fields and temperature. Due to circumferential and axial symmetry of the disc, only half thickness of the disc is used axially, and 15.65° is used circumferentially in finite element analysis by ANSYS. The results show maximum temperature and compressive stress components at the surface and these affects tribological properties such as damage and failure at the surface of the disc. In addition, it was found that high thermal load leads to brake fade and low fatigue life time of cast iron due to surface rupture of the rotor. Good agreement was obtained between FEM and analytical analysis braking cycles to failure.

Key words: Analytical analysis, Heat flux, Finite element method, Stress components,

Acknowledgement

During the course of my thesis work, there were many people who were instrumental and morally helping me. Without their guidance, help and patience, I would have never been able to accomplish the work of this thesis. I would like to take this opportunity to acknowledge some of them.

I am grate full and would like to express my sincere gratitude to my supervisor Dr. Daniel Tilahun for his germinal ideas, invaluable guidance, continuous encouragement and constant support in doing this thesis possible. I appreciate his consistent support from the first day I applied to graduate program to these concluding moments. I am truly grateful for his progressive vision about my training in science, his tolerance of my naïve mistakes, and his commitment to my future career. I also sincerely thanks for the time spent proofreading and correcting my many mistakes.

I am grateful to all staff of Bishoftu Automotive Industry Specially, I want to express my sincere appreciation and gratitude to Mr. Minilik Tekalign and Mr. Biniam Hailimariam for their valuable advice and for always having time for discussions.

I would like to take this opportunity to thank my father and my mother for all their help and understanding. Without my family's encouragement, love and support, this work would never have been accomplished.

Last but certainly not least, I would like to thank all of my friends for their encouragement, and support with different materials and ideas.

List of Tables

List of Figures

Nomenclature

k	Thermal conductivity
δ	Disc thickness
ρ	Density
c	Specific heat
ν	Poisson's ratio
α	Thermal expansion
E	Elastic modulus,
μ	Coefficient of friction μ
p	Hydraulic pressure
ϕ_o	The cover angle of pad in degrees
r, z, θ	Radial circumferential and axial coordinate
δ_d	Disk thickness
δ_p	Pad thickness
R_p	External radius of the pad
r_d	Internal radius of the disk
R_d	External radius of the disk
M	Total mass of the vehicle
V_o	Initial speed of the vehicle
m	Amount of the distributed mass on the front axle of the vehicle
ξ_d	Disc thermal effusivity
ξ_p	Pad thermal effusivity
S_p	Frictional contact surfaces of the disc
S_d	Frictional contact surfaces of the pad
γ	Heat partition coefficient
dE	Rate of heat generated due to friction between two sliding components,
V	Relative sliding velocity and
dF_f	Friction force.
dE_p	Amount of absorbed heat by the pad
dE_d	Amount of absorbed heat by disk
ω	Angular velocity of the disc

q_d	Heat flux of disc
q_p	Heat flux of pad
q_{0d}	Heat flux of disc at t=0 sec.
t_b	Braking time
h	Convection coefficient
T_i	Initial temperature
T_∞	Ambient temperature
σ	Stefan-Boltzmann constant
ε	Emissivity of the surface
α_d	Thermal diffusivity of disc
λ_n	Eigenvalue
$\varphi_n(z)$	Eigen function
Bi	Biot number
ε_t	Thermal strain
σ_r	Normal stress in radial direction.
σ_θ	Normal stress in circumferential direction
σ_z	Normal stress in axial direction.
$\tau_{r\theta}$	Shearing stress in r θ plane
τ_{rz}	Shearing stress in r z plane
$\tau_{r\theta}$	Shearing stress in z θ plane
F_r	Component of the body forces in the radial direction
F_θ	Component of the body forces in the tangential direction
F_z	Component of the body forces in the tangential direction
α	The coefficient of t he linear thermal expansion
ν	The Poisson's ratio
G	Shear modulus
ΔT	Temperature change from the reference temperature T_o

ε_r	Radial deformation strain
ε_θ	Circumferential deformation strain
ε_z	Axial deformation strain
γ_{rz}	Shear deformation strain

Chapter One: Introduction

1.1 Background

A brake disc rotor is the rotating part of a disc brake assembly normally located on the front axle which is most important safety feature of an automobile. The ability of a braking system to provide safe, repeatable stopping is the key to safe motoring. To stop the wheel, friction material in the form of brake pads (mounted in a device called a brake caliper) is forced hydraulically, against both sides of the disc. The purpose of friction brakes is to decelerate a vehicle by transforming the kinetic energy of the vehicle to heat, via friction, and dissipating that heat to the surroundings. So friction based braking systems are still the common device to convert kinetic energy into thermal energy, through friction between the brake pads and the rotor faces. Braking system is performed by combination of different components of disc brake assembly such as caliper, piston and cylinder, pads, and rotor (figure 1.1)

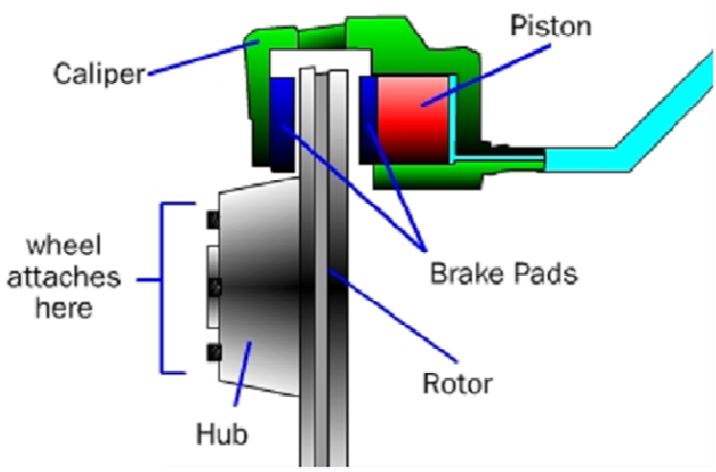

Figure 1.1 Disc brake parts

Based on the design configurations, vehicle friction brakes can be grouped into drum and disc brakes. The drum brakes use brake shoes that are pushed in a radial direction against a brake drum. The disc brakes use pads that are pressed axially against a rotor or disc. Under extreme conditions, such as descending a steep hill with a heavy load, or repeated high-speed decelerations, drum brakes would often fade and lose effectiveness. Compared with their

counterpart, disc brakes would operate with less fade under the same conditions. An additional advantage of disc brakes is their linear relationship between brake torque and pad/rotor friction coefficient. Advantages of disc brakes over drum brakes have led to their universal use on passenger-car and light-truck front axles, many rear axles, and medium-weight trucks on both axles.

Disc-style brakes development and use start at England in the 1890's which is the first ever automobile disc brakes were patented by F.W. Lanchester [1]. It was patented at Birmingha factory in 1902, though it took another half century for the innovation to be widely adopted. The first designs resembling modern style disc brakes began to appear in Britain in the late 1940 and early 1950. The first appeared on the low volume Crosley Hotshot in 1949, although it had to be discontinued in 1950 due to design problems. Modern style disc brakes offered much greater stopping performance than comparable drum brakes, including much greater resistance to "brake fade" which is caused by the overheating of brake components. Meanwhile, from the late 1990 to present, North American automotive industry accelerated the pace on brake research and application to catch up with Japanese quality performance. It has been more tailored towards American vehicle brake designs which often have more challenges to balance between the brake performances and quality [2].

Disk brakes were most popular on sport cars when they were first introduced, since these vehicles are more demanding about brake performance. Disks have now become the more common form in most passenger vehicles.

1.2 Motivation

Excessive thermal deformation of cast iron rotors is one of the most serious problems facing automotive brake designers as they try to enhance disc brake performance for faster and heavier vehicles within tight packaging constraints. In addition, cracking sometimes occurs as a result of repeated high speed stops when the brake rotor is subject to rapid and severe thermal cycling.

The thermal structural analysis is a primordial stage in the study of the brake systems, because the temperature determines thermomechanical behavior of the structure. In the braking phase, temperatures and thermal gradients are very high which produces high

thermal stress. This generates disc thickness variations and deformations whose consequences are manifested by the appearance and the accentuation of cracks. Under the influence of temperature, the friction elements hence, the conditions of operation of the friction patches become less favorable: their wear intensifies and the friction coefficient decreases, material strength decrease due to thermal stress which may lead to emergency situations. Thus, experimental, mathematical and software modeling of the temperature is the important problem at a design stage of brake systems.

This study tries to presents the result comparison of analytical and ANSYS 14.0 and carry out a concise summary of the information about the tensile, compressive, axial, and von mises stress developed during braking. The front disc brake of Huanghai SUV car of model DD6470C will be used for analysis. Due to sliding of disc and pad with each other wear is developed, which is not included in the analysis. The temperature field is obtained considering constant angular velocity, which means heat flux applied on disc surface is constant. Temperature variation occurs only along thickness of the disc, so that thermal and structural analysis is focused only along the thickness of the disc. The material properties are assumed to be temperature independent. Only areas which are exposed to high thermal stress are selected for analysis, which excludes vanes and hub of the disc. Only thermal stresses were considered because the mechanical loads due to the pad normal pressure, centrifugal force and inertia force are insignificant in comparison [3].

1.3 Statement of the Problem

There were so many researches done on transient thermal-structural analysis of disc brake, which are described in literatures. Most of the researches are concentrated on analytical (theoretical method), experimental or finite element method. In each study only one of the methods was applied, which is not satisfactory for accuracy of the analysis. But, this thesis is done both analytical and by finite elements which strengthens the result obtained.

Experimental analysis is accurate as far as instruments are fully available, sufficient knowledge of using instruments, and good conditions to apply instruments. And this is difficult to estimate thermal structural analysis between disc and pads, where there is heat dissipation over time and high speed rotation of disc. Experimental determination of temperature and stress of a surface of

contact concerning authentic objects in most cases causes significant technical difficulties and is connected with essential material and time expenses. Instruments which pass these obstacles face another obstacle which is expensiveness of these instruments. Taking this in to consideration, the aim of this paper is studying and comparing analytical analysis and finite element /ANSYS software analysis of a temperature and stress along the thickness of the front disc brake. This is done by applying mathematical analysis of heat transfer and stress boundary conditions.

1.4 Objective of the Study

Main Objective

The main objective of the thesis work is to study analytical analysis and finite element analysis of thermal stress distribution in disc thickness caused by temperature distribution, and its effect on life and brake fading.

Specific Objective

- ✓ Developing thermal boundary condition and thermal equation governing temperature distribution through the disc thickness
- ✓ 3-D modeling of disc brake using ANSYS 14.0 software to study temperature distribution through thickness of the rotor
- ✓ Comparing analytical and ANSYS temperature distribution to check whether input for thermal stress is same or not for analytical and finite element method (ANSYS)
- ✓ Developing analytical transient thermal stress using constrained boundary conditions
- ✓ Using symmetry boundary condition of 3-D modeled brake rotor to simplify the analysis
- ✓ Analysis of thermal stress components by finite element method (ANSYS) using temperature developed as an input parameter

1.5 Organization of the Thesis

This thesis is organized in to six chapters. In the first chapter, background and justification of this thesis work and the objectives to be achieved are discussed. In chapter two, a review of literature relevant to this thesis work, which has been investigated by different researchers, is given. Chapter three is about analytical method in temperature and thermal stress analysis. In chapter four, finite element method (FEM) is used, to develop 3-D model of disc brake. Also

different thermal and structural boundary conditions are discussed in detail. In addition application of symmetry is justified here. In chapter five results of the analysis are summarized and discussions are made based on the outputs of the FEM. In addition, comparison of analytical and numerical solutions is made. Finally, chapter six gives conclusion achieved from this thesis work and propose future work in this field of study.

Chapter Two: Literature Reviews

Due to the application of brakes on the car disk brake rotor, heat generation takes place due to friction and this thermal flux has to be conducted and dispersed across the disk rotor cross section. The condition of braking is very much severe and thus the thermal and structural analysis has to be carried out. Taking this in to consideration, many researchers have been done about the brake disc thermo-mechanical coupling analysis.

S. Koetniyom [4] Studied thermal stress analysis of automotive disc brakes to develop material properties of gray cast cast iron brake disc model of the Rover disc subjected to severe thermal cycles using the commercial package ABAQUS. One particular existing brake disc design for a medium passenger car was chosen for the investigation. Due to symmetry, the final model of the disc was a 20° segment of the brake disc and hub meshed using nearly three thousand 20 noded solid elements with a quadratic interpolation function. In addition, experimental work was undertaken to derive the rotor material properties in tension and compression as a function of temperature. This data was used to generate suitable FE material model routines which accurately allow for the different temperature dependent yield properties of cast iron in tension and compression. Using the most accurate user developed material subroutine, the thermal response of the back-and front-vented disc designs are compared: the back-vented disc suffers lower thermal distortion but at the expense of higher plastic strain accumulation, particularly near the point of attachment of the vanes. The result indicates that temperatures increase non-uniformly with the braking time and the disc is subjected to maximum temperatures up to around 380 °C at the end of the brake application. Thermal stress result shows maximum von Mises elastic stresses at the neck was 273 MPa and near the inner fillet radius of the long vane 442 MPa due to the constraints applied to the free expansion of the rotor rubbing surfaces. If these stresses arc beyond the proportional limit, plastic strains would occur in the brake disc.

Hogskolan [5] studied simulation of thermal fatigue stresses in a disc brake by taking as an input the heat flux produced from the friction between a disc and pad system for a number of repeated braking cycles. He used the finite element analysis (FEA) to determine the temperatures

profile in the disc and to analyze the stresses for the repeated braking, which could be used to calculate the fatigue life of a disc. Sequentially coupled approach was used for thermo-mechanical problem and the problem was divided into two parts, heat analysis and thermal stress analysis. The heat analysis was obtained by including frictional heat and adopting an Eulerian approach. The thermal stress analysis, which was the main focus of his thesis, was followed using Abaqus. The plasticity theory as background for stress analysis was discussed in detail and temperature independent material properties were considered throughout the thesis work. The linear kinematic hardening model with rate independent elastic-plastic plasticity is used for benchmark and real disc-pad model. The results of the benchmark model and the real model were observed to be similar in terms of plasticity theory. First brake application stays for 6 second, and the result shows maximum temperature of 220^{o}C at 2.5 seconds. After first brake application mean equivalent stress of 180Mpa was shown.

Samic and Sheridan [6] investigated the effects of friction on the pressure distribution between the rotor and the pads with a floating caliper using the finite element technique. The computational results without the friction forces (static case) revealed that the inboard and outboard pressure distributions varied because the locations of the normal forces acting on the pads were different on the piston and finger sides of the floating caliper. Furthermore, the pressure distributions with the friction forces taken into account were different from the static case due to the moment set up between the abutment and the friction interface.

Similarly, Lee et al. [7] studied the pressure distribution between the rotor and the pads including the friction force with a floating caliper in order to investigate the motion at the friction interface that could be used to determine the onset of disc brake squeal using the finite element technique. The computed result revealed that the pressure distributions acting on the pads were different on the piston and finger sides of the floating caliper. Moreover, the axial displacements at the friction interface on the two sides were different.

The heat flux generated at the rubbing surface can transfer to both the rotor and the pad. The amount of thermal energy transferred into the brake rotor depends on the specification of the friction and disc materials. Yano and Murata [8] performed experimental work to determine the amount of heat flow from the frictional interface into the rotor by conduction. The volume or quantity of heat transferring to the pads, the rotor and the ambient air was obtained

from the measured temperature gradients and heat transfer coefficients. According to their experiments, the heat conduction from the rubbing surfaces to the rotor was approximately 72% of the heat generated.

Belhocine and Bouchetara [17] studied simulation of fully coupled thermomechanical analysis of disc brake rotor caused by frictional heat generated during braking application. They studied surface roughness and wear at the pad interface using finite element method by building 3D model of ventilated pad-disc brake assembly with a thermomechanical coupling boundary condition and multi-body model technique. The numerical simulation for the coupled transient thermal field and stress field was carried out by sequentially thermal structural coupled method based on ANSYS to evaluate the stress fields and of deformations which were established in the disc had with the pressure of the pads and in the conditions of tightening of the disc thus the contact pressures distributions field in the pads which was another significant aspect in their research paper. In addition effects of materials on mechanical properties are studied by using three different types of gray cast iron materials.

Noyes and Vickers [10] predicted the temperature response on the rubbing surfaces of a brake disc, using the assumption of a uniform heat flux. The computational results were compared with the temperatures measured at the rotor surface on entry to and exit from the pad area. It was found that the measured temperature on exit from the pad was higher than the temperature calculated using the assumption of uniform heat flux by approximately 55°C. However, for many applications, the effect of this circumferential temperature variation, the so-called "rotating heat source" effect, can be ignored.

J. G. Balotin [11] studied analysis of the influence of temperature on the friction coefficient of friction materials. He tried to verify the behavior of the friction coefficient when the friction material is submitted to high temperature brakings (stage also known as Fade). The experiments were performed in three distinct stages: bedding-in, characterization and fade. Three sets of twelve brakings were performed for friction characterization. He founded that the fade stages degrade the phenolic resins of the materials and affect the performance of the friction material. The test results of his paper show that brake pads with different formulations have a variation on the performance of friction coefficient with brakings at high temperatures (fade), which is decrease of coefficient of friction with increase of temperature which leads to brake fade.

Nakatsuji et. al. [12] did a study on the initiation of hair-like cracks which formed around small holes in the flange of one-piece discs during overloading conditions. The study showed that thermally induced cyclic stress strongly affects the crack initiation in the brake discs. Using the finite element method, the temperature distribution under overloading was analyzed. 3D unsteady heat transfer analyses were conducted using ANSYS. A 1/8 of the one piece disc was divided into finite elements, and the model had a half thickness due to symmetry in the thickness direction.

Babukanth and Vimal [13] studied transient Analysis of disk brake using ANSYS Software by choosing element type solid 90, which is higher order version of the 3-D eight node thermal element (Solid 70). The element has 20 nodes with single degree of freedom, temperature, at each node. The 20-node elements have compatible temperature shape and are well suited to model curved boundaries. The 20-node thermal element is applicable to a 3-D state or transient thermal analysis. If the model containing this element is also to be analyzed structurally, the element should be replaced by the equivalent structural element (Solid 95)

Recent numerical models, presented to deal with thermal stress [14,15] have shown that the thermal gradients can attain important levels which depend on the heat dissipated by friction, the sliding speed and the heat convection coefficient. Many other works dealt with the evaluation of temperature in solid disks subjected to frictional heating. The temperature distribution due to friction process necessitates a good knowledge of the stress parameters. In fact, the interface is always imperfect due to the roughness from a mechanical and thermal point of view.

In the scope of the present work both finite element method and analytical analysis are done and compared. None of the above approaches were available found to be fully compared with other result. In some cases the geometry boundary conditions were inappropriate; in others the published information was insufficient to allow direct implementation. As a result, it is decided to develop a new solution to meet our requirements; this is presented in the following chapters.

Chapter Three: Analytical Analysis Methods and Conditions

3.1 Gray Cast Iron Material Composition and Thermoelastic Properties

A disk brake rotor is generally made from gray cast iron due to cast iron provides good wear resistance with high thermal conductivity, high thermal diffusivity, and low production cost compared to other disc brake rotor materials such as AL-MMC (Aluminum metal matrix composite), carbon composites and ceramic based composites [16]. Due to this reason it is a material that has been commonly used to create components of varying complexity for a long time. Gray iron's high damping capacity, combined with its excellent machinability and high hardness, is unique to this material and makes it ideally suited for machine bases and supports, engine cylinder blocks and brake components (table 3.1).

Table 3.1 Gray Cast Iron Specifications, Characteristics & Applications

Standard Specifications	Characteristics	Applications
✓ ASTM A48: gray iron castings ✓ ASTM A74: cast iron soil & pipe fittings ✓ ASTM A126: gray iron castings for valves, flanges & pipe fittings ✓ ASTM A159: automotive gray iron castings ✓ SAE J431: automotive gray iron castings	✓ Several strength grades; ✓ Low rate of thermal expansion ✓ Resistance to thermal fatigue; ✓ Lubrication retention; and good machinability.	✓ Automobile engine blocks & heads, clutch; ✓ Internal combustion engines ✓ machine tool bases; ✓ Brake components

Excessive vibration causes inaccuracies in precision machinery and excessive wear on gear teeth and bearings. The damping capacity of gray iron is considerably greater than that of steel and other iron types. For example, if gray iron, CGI (compacted graphite iron and ductile iron) and ductile iron have a similar composition, the relative damping capacity of gray iron is 1.0, CGI is 0.35 and ductile iron is 0.14. The damping capacity of gray iron is about 20-25 times higher than steel.

The properties of gray iron are primarily dependent on its composition. Normally, cast iron consists of two main substances: graphite (carbon) flakes and matrix ferrous metal. Both of

these constituents have a significant influence on the stress-strain response of the material. This is because of the weak bonding between the graphite flakes and metal matrix which causing gaps or voids to open in the material under tension. Therefore, the compressive strength of cast iron is two or three times higher than its tensile strength, even though isotropic material property is used in this thesis [17]. In order to capitalize on this condition, the cast iron product should be designed to be loaded in compression wherever possible. The presence of the graphite provides several valuable characteristics to cast iron. These include:

- ✓ The ability to produce sound castings economically in complex shapes such as water cooled engine blocks.
- ✓ Dimensional stability under differential heating such as in brake drums and disks.
- ✓ High vibration damping as in power transmission cases, and brakes
- ✓ Border line lubrication retention as in internal combustion engine cylinders

Iron accounts for more than 95%, while the main alloying elements are carbon and silicon. Cast irons contain appreciable amounts of silicon, and consequently these alloys should be considered ternary Fe-C-Si alloys. Appreciable silicon content is necessary in gray iron because this element causes the precipitation of the graphite in the iron. Silicon also imparts corrosion and elevated temperature oxidization resistance to gray iron. Here graphite is present in the form of flakes.

To classify gray iron in accordance to its thermoelastic properties, ASTM (American Standard of Testing Material) Standard A48 and SAE (Society of Automotive Engineer) Standard J431 provide the best details to accomplish this task. The two specifications approach the task from different standpoints but essentially the concept remains the same. For example, the number in a Class 30 gray iron refers to the minimum tensile strength in ksi. Class 30A indicates that the iron must have a 30 ksi (207 MPa) tensile strength in an “A” bar (0.875in. as cast diameter). In SAE Standard J431, tensile strength is not required, but hardness and a minimum tensile strength to hardness ratio are required. The class then is identified as a grade.

Properties of gray cast iron materials were adopted from the previous study of Belhocine and Bouchetara [17] which are related to SAE or ASTM specification (table 3.2 and table 3.3).

Table 3.2 Mechanical properties of the disc and pad

Density, ρ (kg/ m^3)		Poisson's Ratio, v		Tensile Strength of Disc, σ_y (Mpa)	Modulus of Elasticity, E of Disc (Gpa)	Compression to Tensile Strength Ratio of Disc	Brinell Hardness of Disc	Coefficient of Friction, μ Between Disc-pad Contact
Disc	Pad	Disc	Pad					
7250	1400	0.28	0.25	206	130	3.84	220	0.35

The SAE maintains specifications for various applications such as brake drums, disc and clutch plates to resist thermal shock for the manufacture of grey iron (table 3.1). For normal car and light truck applications, the SAE specification for GG25 is J431. This specification dictates the correct range of hardness, chemical composition (Carbon 3.20-3.50%, Silicon 1.90-2.30%, Manganese 0.60-0.90%, Sulfur (0.02-0.25%), Phosphorus (0.02-1%)), tensile strength, and other properties necessary for the intended use. There are no generally accepted standard for surface finish, machining allowance, or dimensional tolerances. The table 3.2 shows properties of gray cast iron with high carbon content, with good thermophysical characteristics and the brake disc has an isotropic elastic behavior.

Table 3.3 Thermal properties of disc and pads

Thermal Properties	**Pad**	**Disc**
Thermal conductivity, k (w/m.^{o}C)	5	57
Specific heat, c (J/kg.^{o}C)	1000	460
Thermal expansion α, 10^{-6}/^{o}C	10	10.85

The thermal structural stability of the disc brake is influenced by the thermal and elastic property of cast iron materials, rate of hydraulic pressure applied on pad and the basic design for the disc rotor. Some of the thermally most important properties of disc brake rotor are as follows [18]:-

- ✓ Thermal capacitance (density and specific heat) is the ability to store the heat. Initially on braking process, a significant amount of frictional heat is stored and during short braking, this thermal capacitance is dominates.

- ✓ Thermal conductivity is the ability to re-distribute the thermal energy. During long and low intensity braking, the peak temperature is largely depends on the disc material's conductivity. However, the thermal conductivity has a little effect during short braking.
- ✓ Thermal expansion coefficient (related to location of friction contact due to the thermal deformation) affects the tendency towards hot spotting and thermal disc thickness variation (DTV) generation. The temperature gradients of the disc brake can cause to temporary DTV owing to the uneven thermal expansion of the material

3.2 Analytical Analysis Conditions

For comparison of thermal structural analysis between analytical and finite element, the dimensions and specifications of SUV (Sport Utility Vehicle) car of model DD6470C is selected. The detail of this specification is in appendix I. Dimensions and specifications of this car are taken from Bishoftu Automotive Industry. SUV car is manufactured by Huanghai Company in China, and Bishoftu Automotive Industry imports the disassembled parts and assembles it locally. The demand of this car is increasing worldwide due to its quality in fuel economy, less expensive, and varying amount of towing capacity with an all-wheel drive or four wheel drive system. The maximum high speed set for this car is as high as 36m/s which is higher than pick-up car (30m/s). This high speed makes this car to be selected for the analysis of thermal structural-structural analysis of its disc brake.

Figure 3.1 Huanghai SUV car of model DD6470C

They also provide extra traction in slippery conditions and the ability to tackle at least moderate off-road terrain. Taking these in to consideration Bishoftu Automotive Industry imported the

disassembled parts from Huanghai Company. The demand of this car is highly increased now days in government officials, as well as in private company.

Figure 3.2 Measuring dimensions of disc and pad

3.2.1 Geometries and Dimensions of Brake Disk-pad

Dimensions of disc and pads are used for development of 3-D drawing. Radius and thickness, as well as other complex structures are used as an input for analysis. These dimensions are taken by measuring the disc by caliper. In addition maximum speed is used for thermal analysis. This and other necessary data are found on SUV specification (appendix I).

Table 3.4 Measured dimensions of disc rotor and pad

Symbols	Meaning	Value
ϕ_o	The cover angle of pad (in degrees)	65
r, z, θ	Radial circumferential and axial coordinate	-
r_p	The internal radius of the pad, mm	60
R_p	External radius of the pad, mm	120
r_d	Internal radius of the disk, mm	60
R_d	External radius of the disk, mm	120
δ_d	Disk thickness, mm	24
δ_t	Vent thickness	6
δ_p	pad thickness, mm	12

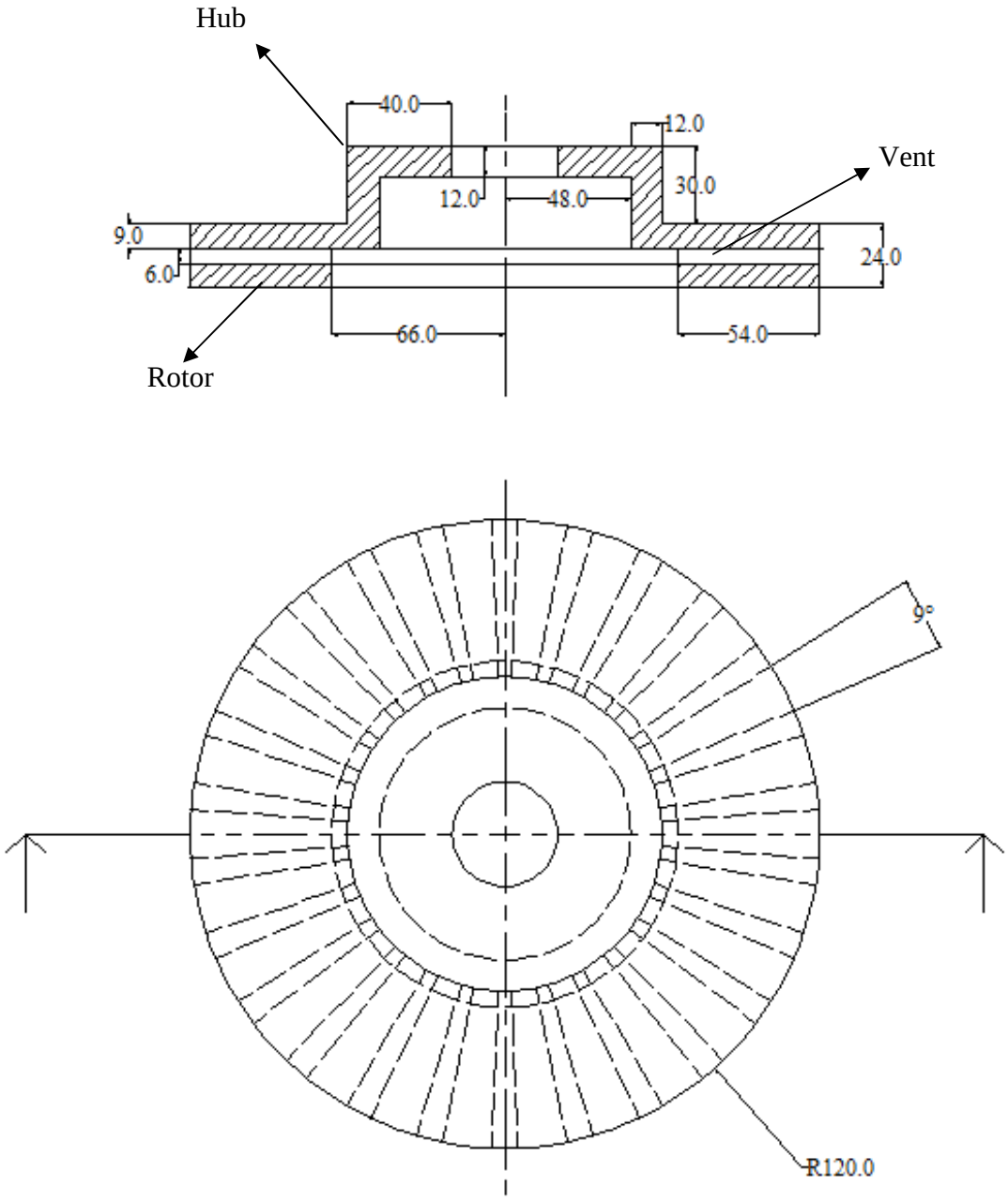

Figure 3.3 Cross sectional view of the disc

The values displayed in table 3.4 are found on figure 3.3 and figure 3.4. This thesis is focused on a study of ventilated disc brake rotor of SUV Huanghai vehicle with full load of capacity with selected positions for study of thermal stress analysis. Therefore only thickness of a rotor is the main concentration of this thesis. Cylindrical cordite system is used to describe the dimensions. Different surfaces of disc or pad shown in figure 3.4 are designated by the following symbols.

Ω_1 Contact surface area between pads and disc (upper)

Ω_2 External radius surface area

Ω_3 Internal radius surface area

Ω_4 Contact surface area between pads and disc (lower)

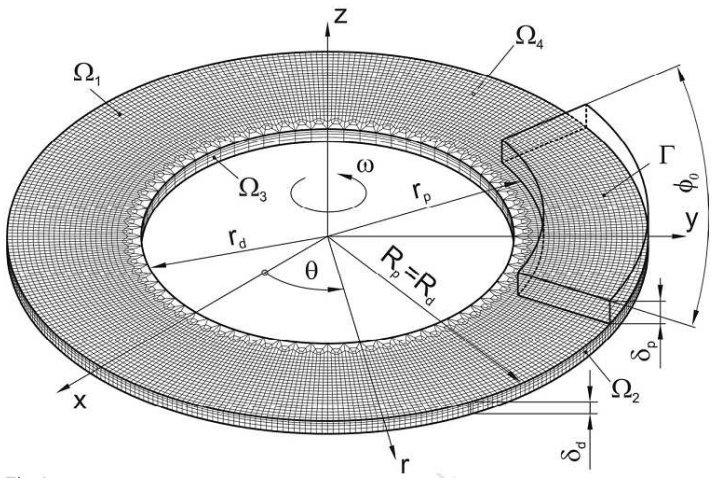

Figure 3.4 Dimensioning disc and pad

3.2.2 Thermal Loading and Boundary Condition

Based on the information of the Vehicle Research & Test Center of Huanghai SUV car specification (appendix I), the average of stopping distance with fully loaded disc brake (30^0C ambient temperature) traveling at a speed of 130 km/hr (36m/s) under the roller test conditions, required an average of 81m stopping distance with the deceleration rate 8 m/s^2 in 4.5 second. For the analysis, speed of the car reduced from 36m/s to zero within 4.5 seconds (figure 3.5). In this thesis, the single stop cycles of braking were used to analyze thermal structural analysis, because the material regains its original condition (elastic) after force is removed.

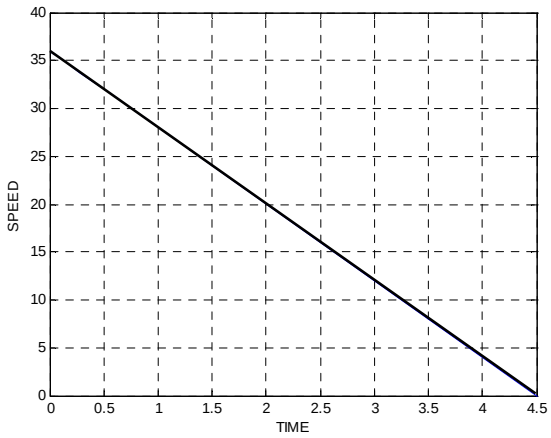

Figure 3.5 Braking conditions

In actually, variation of the rotating speed during braking must be determined through vehicle dynamics. However, in this study, the rotating speed of disk was considered to be a 300rad/sec. at t=0, which is maximum speed divided by external radius of disk. The final velocity is zero. For the purpose of comparison of obtained results, pressures of 1Mpa are taken from specification of the SUV car (appendix I). The heat dissipated through the brake disc surface during the heat flux applied to the both surface are ignored and only can be considered during the idle time.

Heat transfer convection is only considered after brake application is completed, and the car accelerated to regain its original speed. The remaining surface area of the disc is considered to be insulated. These areas include circumferential areas, inner and external radius areas of the disc. They are several assumptions have been made to simplify the analysis complexity and at the same time allow the reasonable output is obtained from the result of the analysis. In the temperature analysis for repeated braking,

- ✓ Material properties are isotropic and independent of the temperature
- ✓ The nominal surface of contact between the disc brake and the pad in operation is equal to the apparent surface in the sliding motion.
- ✓ The contact pressure is uniformly distributed over all friction surfaces hence the heat generation of the midplane is considered as symmetric

- ✓ Radiation is neglected by virtue of short braking time and hence relatively low temperature
- ✓ The wear on the contact surface is negligible.
- ✓ Temperature vary only along thickness and constant heat flux is applied radially

The differential equation of heat conduction will have numerous solutions unless a set of boundary conditions and an initial condition (for the time-dependent problem) are prescribed. Boundary conditions specify the temperature or the heat flow at the boundaries of the region. For example, at a given boundary surface, the temperature distribution may be prescribed, or the heat flux distribution may be prescribed, or there may be heat exchange by convection and/or radiation with an environment at a prescribed temperature. The boundary condition can be derived by writing an energy balance equation at the surface of the solid.

We consider a surface element having an outward-drawn unit normal vector **n**, subjected to convection, radiation, and external heat supply as illustrated in figure 3.6. The physical significance of various heat fluxes shown in this figure is as follows.

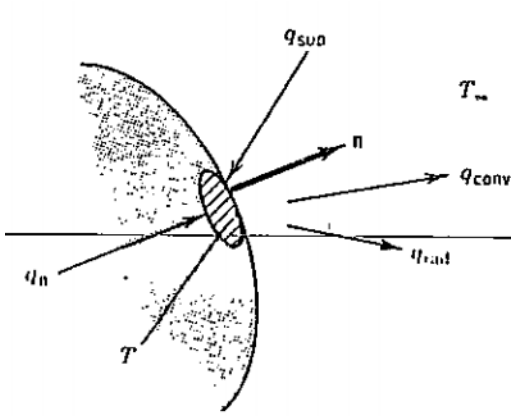

Figure 3.6 Energy balance at the surface of a solid parts

The quantity q_{sup} represents energy supplied to the surface, in W/m^2, from an external source.

The quantity a q_{conv} represents heat loss from the surface at temperature T by convection with a heat transfer coefficient h into an external ambient at a temperature T_∞, and is given by

$$q_{conv} = h(T - T_\infty) \quad W/m^2 \quad \text{…….. 3.1}$$

Here the heat transfer coefficient h varies with the type of flow (laminar, turbulent, etc.), the geometry of the body and flow passage area, the physical properties of the fluid, the average temperature, and many others.

The quantity q_{rad} represents the heat loss from the surface by radiation in to an ambient at an effective temperature T, and is given by

$$q_{rad} = \varepsilon\sigma(T^4 - T_\infty{}^4) \quad \text{…….3.2}$$

Where ε is the emissivity of the surface and σ is the Stefan-Boltzmann constant, that is, σ =5.6697 x 10^{-8} W/(m^2.K^4).

The quantity q_n represents the component of the conduction heat flux vector normal to the surface element and is

$$q_n = -k\frac{\partial T}{\partial n} \quad \text{……..……....3.3}$$

To develop the boundary condition, we consider the energy balance at the surface as

Heat supply = heal loss

$$q_n + q_{sup} = q_{conv} + q_{rad} \quad \text{.....…….3.4}$$

Introducing the expressions 3.1, 3.2, and 3.3 into 3.4, the boundary condition becomes

$$-k\frac{\partial T}{\partial n} + q_{sup} = h(T - T_\infty) + \varepsilon\sigma(T^4 - T_\infty{}^4) \text{.....3.5a}$$

$$k\frac{\partial T}{\partial n} + hT + \varepsilon\sigma T^4 = q_{sup} + hT_\infty + \varepsilon\sigma T_\infty{}^4 \text{.....3.5b}$$

Where all the quantities on the right hand side of equation 3.5b are known and the surface temperature T is unknown. The general boundary condition given by equations 3.5b is nonlinear because it contains the fourth power of the unknown surface temperature T^4. In addition, the absolute temperatures need to be considered when radiation is involved.

In this thesis, for the analytic solution of linear heat conduction problems, three different types of linear boundary conditions are considered: boundary condition of the first kind, second kind and third kind.

Boundary condition of the first kind is the situation when the temperature distribution is prescribed at the boundary surface, that is T=f(z, t) on S where the prescribed surface temperature f(z, t) is, in general, a function of position and time. The special case T=0 on S is called homogeneous boundary condition of first kind

Boundary condition of the second kind is the situation in which the heat flux is prescribed at the surface, that is $k\frac{\partial T}{\partial n} = f(z,t)$ on S, where, $\frac{\partial T}{\partial n}$ is the derivative along the outward drawn normal to the surface. Here f(z, t) is the prescribed heat flux, W/m^2. The special case $\frac{\partial T}{\partial n} = 0$ on S is called the homogeneous boundary condition of the second kind.

Boundary condition of the third kind is the convection boundary condition which is readily obtained from equation 3.5b by setting the radiation term and the heat supply equal to zero, that is $k\frac{\partial T}{\partial n} + hT = hT_{\infty}(z,t)$ on S. where, for generality, the ambient temperature T_{∞}(z, t) is assumed to be a function of position and time. The special case

$k\frac{\partial T}{\partial n} + hT = 0$ On S is called the homogeneous boundary condition of the third kind. It represents convection into a medium at zero temperature.

Figure 3.7 shows the boundary conditions of the disk for two types of pressure distribution; uniform wear and uniform pressure in figure a and b respectively. As it can be seen, since the thermal problem in the disk is symmetric in z direction, only the half of the disk (z=δ/2) is considered. So the transient heat equation for the disk and the related boundary conditions that have been shown in the figure is formulated as follows.

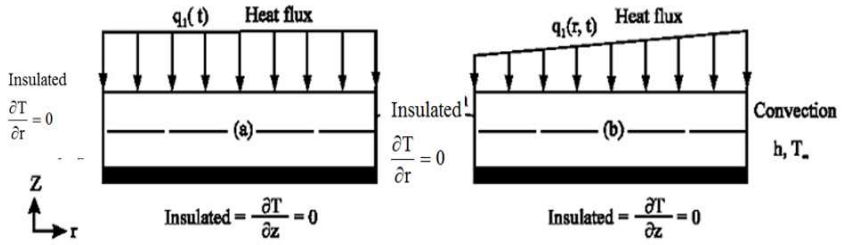

Figure 3.7 Boundary condition of the disk (a) uniform wear (b) uniform pressure

The location of first boundary condition on rotor is found at z=0, which is insulated surface. It is homogeneous boundary condition of the second kind (special case). This boundary condition is resulted due to axial symmetry (half thickness of the disc).

$$\frac{\partial T}{\partial z} = 0 \quad \text{.....3.6a}$$
$$z = 0$$
$$r_d \le r \le R_d$$
$$t \ge 0$$

The second boundary condition is found at z=δ (surface of the rotor). This boundary should be considered in two sections, one of them is exposed to the boundary condition of the third kind or convection, and the other is exposed to the boundary condition of the second kind, or prescribed heat flux. Heat flux is specified in contact zone of disk-pad due to the frictional heating between the pads and disk. Boundary condition of the third kind is ignored here due to first brake application.

$$\frac{\partial T}{\partial z} = q_o \quad \text{.....3.6b}$$
$$z = \delta$$
$$r_d \le r \le R_d$$
$$t \ge 0$$

With initial condition of

$$T(r, z, 0) = T_o \qquad r_p \le r \le R_p \qquad 0 \le z \le \delta_p \quad \text{.....3.6c}$$

3.2.3 Solid Mechanics Aspect and Structural Boundary Condition

Thermal stresses are defined as self balancing stresses produced by a non-uniform distribution of temperature or by differing coefficients of thermal expansion [19]. These thermal stresses are developed in a solid body whenever any part is prevented from assuming the size and shape that it would freely assume under a change in temperature. Time dependent thermal boundary conditions are assumed to act on the disc surfaces axially. The transient temperature response of the brake disc is first required in order to be used as a load input for the thermal stress analysis. In the first step, the general relation and analytical solution for the temperature distribution is derived by means of dimensionless parameter followed by separation of variables in disc thickness using transient dimensionless variable. In second step the thermal stress components are extracted by means of the displacement technique applied to a one dimensional problem of disc bodies. Specific solutions were determined for the case of transient thermal loading case applied to disc.

One of the causes of initial stresses in a body is no uniform heating. With rising temperature the elements of a body expand. Such an expansion generally cannot proceed freely in a continuous body, and stresses due to the heating are set up. In many cases of machine design, such as in the design of brakes, steam turbines and diesel engines thermal stresses are of great practical importance and must be considered in more detail. Solution of thermal stress problems requires reformulation of the stress-strain relationships accomplished by superposition of the strain attributable to stress and that due to temperature. For a change in temperature T(z), the change of length δL, of small linear element of length L in an unconstrained body is $\delta L = \alpha LT$. Here α, is the coefficient of linear thermal expansion. The thermal strain ε_t associated with the free expansion at a point is then

$$\varepsilon_t = \alpha T \quad \ldots\ldots\ldots\ldots\ldots\ldots\ldots\ldots\ldots\ldots\ldots\ldots 3.7$$

To ascertain the distribution of stress, strain, and displacement with in an elastic body subjected to a prescribed system of forces requires consideration of a number of conditions relating to certain physical laws, material properties, and geometry. These fundamental principles of

analysis also referred to as the three aspects of solid mechanics problems: Condition of equilibrium, condition of compatibility and

Condition of equilibrium is related to statistics equation. The equation of statistics must be satisfied throughout the body. The stress field in an elastic solid is continuously distributed within the body and uniquely determined from the applied loadings. Because we are dealing primarily with bodies in equilibrium, the applied loadings satisfy the equations of static equilibrium; that is, the summation of forces and moments is zero. If the entire body is in equilibrium, then all parts must also be in equilibrium. Thus, we can partition any solid into an appropriate subdomain and apply the equilibrium principle to that region. Following this approach, equilibrium equations can be developed that express the vanishing of the resultant force and moment at a continuum point in the material. These equations can be developed by using either an arbitrary finite subdomain or a special differential region with boundaries coinciding with coordinate surfaces.

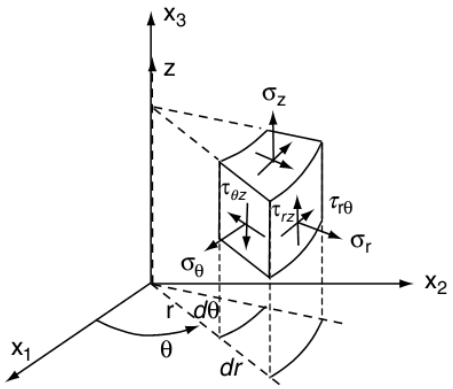

Figure 3.8 Stress components in cylindrical coordinates.

In order to solve many elasticity problems, formulation must be done in curvilinear coordinates typically using cylindrical or spherical systems. The stress components are defined on the differential element shown in Figure 3.8, and thus the stress matrix is given by.

$$\sigma = \begin{bmatrix} \sigma_r & \tau_{r\theta} & \tau_{rz} \\ \tau_{r\theta} & \sigma_\theta & \tau_{\theta z} \\ \tau_{rz} & \tau_{\theta z} & \sigma_z \end{bmatrix} \quad \text{.....3.8}$$

Now wish to develop expressions for the equilibrium equations in curvilinear cylindrical and spherical coordinates. By using a direct vector/matrix notation, the equilibrium equations can be expressed as [20]

$$\frac{\partial \sigma_r}{\partial_r} + \frac{1}{r}\frac{\partial \tau_{\theta r}}{\partial \theta} + \frac{\partial \tau_{rz}}{\partial z} + \frac{\sigma_r - \sigma_\theta}{r} + F_r = 0$$
$$\frac{1}{r}\frac{\partial \sigma_\theta}{\partial \theta} + \frac{\partial \tau_{r\theta}}{\partial r} + \frac{\partial \tau_{\theta z}}{\partial z} + 2\frac{\tau_{r\theta}}{r} + F_\theta = 0 \qquad \ldots\ldots\ldots\ldots\ldots\ldots 3.9$$
$$\frac{\partial \tau_{rz}}{\partial r} + \frac{1}{r}\frac{\partial \tau_{\theta z}}{\partial \theta} + \frac{\partial \sigma_z}{\partial z} + \frac{1}{r}\tau_{rz} + F_z = 0$$

σ_r- Normal stress in radial direction.

σ_θ- Normal stress in circumferential direction

σ_z- Normal stress in axial direction.

$\tau_{r\theta}$- Shearing stress in r θ plane

τ_{rz}- Shearing stress in r z plane

$\tau_{r\theta}$- Shearing stress in z θ plane

F_r- Component of the body forces in the radial direction

F_θ- Component of the body forces in the tangential direction

F_z- Component of the body forces in the tangential direction

The second aspect of solid mechanics is condition of compatibility. The geometry of deformation and the distribution of strain must be consistent with the preservation of body continuity. The true solutions satisfy also the compatibility equation (biharmonic equation in polar coordinate):

$$\left(\frac{\partial^2}{\partial r^2} + \frac{1}{r}\frac{\partial}{\partial r} + \frac{1}{r^2}\frac{\partial^2}{\partial \theta^2} + \frac{\partial^2}{\partial z^2}\right)(\sigma_r + \sigma_\theta + \sigma_z + \alpha E T) = 0 \qquad \ldots\ldots\ldots\ldots\ldots\ldots 3.10$$

In addition, the stress, strain, and displacement fields must be such as to conform to the condition of loading imposed at the boundaries. This is known as satisfying the boundary conditions for a particular problem.

The third solid mechanics aspect is condition of Hook's law (stress strain relations). Material properties (constitutive relations, for example, Hook's law) must comply with the known behavior of the material involved. The total r, θ, and z strains ε_r, ε_θ and ε_z are obtained by adding to thr thermal strains of the type described above and the strains due to stress resulting from external forces. From Hook's law for a homogeneous isotropic body in cylindrical coordinate system are [21, 22]:

$$\varepsilon_{rr} = \frac{1}{E}\left[\sigma_{rr} - \upsilon(\sigma_{\theta\theta} + \sigma_{zz})\right] + \alpha\Delta T = \frac{1}{2G}\left(\sigma_{rr} - \frac{\upsilon}{1+\upsilon}\Theta\right) + \alpha\Delta T \quad \text{.....3.11a}$$

$$\varepsilon_{\theta\theta} = \frac{1}{E}\left[\sigma_{\theta\theta} - \upsilon(\sigma_{rr} + \sigma_{zz})\right] + \alpha\Delta T = \frac{1}{2G}\left(\sigma_{\theta\theta} - \frac{\upsilon}{1+\upsilon}\Theta\right) + \alpha\Delta T \quad \text{.....3.11b}$$

$$\varepsilon_{zz} = \frac{1}{E}\left[\sigma_{zz} - \upsilon(\sigma_{rr} + \sigma_{zz})\right] + \alpha\Delta T = \frac{1}{2G}\left(\sigma_{zz} - \frac{\upsilon}{1+\upsilon}\Theta\right) + \alpha\Delta T \quad \text{.....3.11c}$$

And

$$\varepsilon_{r\theta} = \frac{\sigma_{r\theta}}{2G} \quad \text{.....3.12a}$$

$$\varepsilon_{\theta z} = \frac{\sigma_{\theta z}}{2G} \quad \text{.....3.12b}$$

$$\varepsilon_{zr} = \frac{\sigma_{zr}}{2G}, \quad \text{.....3.12c}$$

$$\Theta = \sigma_{rr} + \sigma_{\theta\theta} + \sigma_{zz} \quad \text{.....3.13a}$$

$$G = \frac{E}{2(1+\upsilon)} \quad \text{.....3.13b}$$

$$\Delta T = T(z,t) - T_o \quad \text{.....3.13c}$$

With

E- Young's modulus

α- The coefficient of t he linear thermal expansion

ν – The Poisson's ratio

G- Shear modulus

ΔT is the temperature change from the reference temperature T_o (where the reference temperature can be the temperature of the body in the unstrained state or the ambient temperature before a change of temperature).

Similar to other field problems in engineering science, the solution of thermal stress requires appropriate boundary conditions on the body under study. Thermal boundary conditions are stated in thermal analysis such as insulated surfaces and heat flux boundary conditions. In similar manner there are a number of structural boundary conditions as well as free surfaces from traction. The common types of boundary conditions for thermal stress applications normally include specification of how the body is being supported or loaded. This concept is mathematically formulated by specifying either the displacements or tractions at boundary points. A common example of this situation is shown in disc brake for a case involving a surface of problem symmetry where the condition is one of a rigid-smooth boundary with zero axial and circumferential displacements and zero radial traction. Boundary conditions are normally specified using the coordinate system describing the problem and thus particular components of the displacements and tractions are set equal to prescribed values. For displacement-type conditions, such a specification is straightforward, and a common example includes fixed boundaries where the displacements are to be zero. In general three types of boundary conditions available in this analysis: circumferential, axial and radial constraints.

3.2.3.1 Circumferential Constraint

Circumferential boundary condition is due to geometrical symmetry of the rotor, and shown in figure 3.13 below. When temperature rises, and the material tries to expand freely along circumference, the circumferential compressive stress $\sigma = -\alpha E \Delta T$ suppresses the expansion which means fixed boundaries where the displacements are to be zero. The element can

maintained in this condition by applying the distribution of compressive force given to the edges θ=constant value.

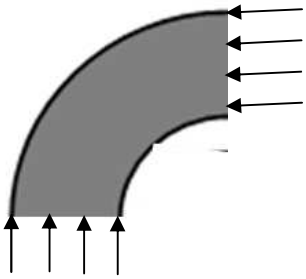

Figure 3.9 Circumferential Constraint (zero displacement)

3.2.3.2 Axial Constraint

Due to application of the pads from both side, free thermal expansion of the rotor in axial direction is suppressed, by compressive force $\sigma_z = -\alpha E \Delta T$ along axial direction, and there are two fixed boundaries where the displacements are to be zero. One is due to symmetry (the lower surface of the disc) and the other is due to pads axial displacement of the rotor (the upper surface of the rotor) is constrained to zero value (figure 3.14).

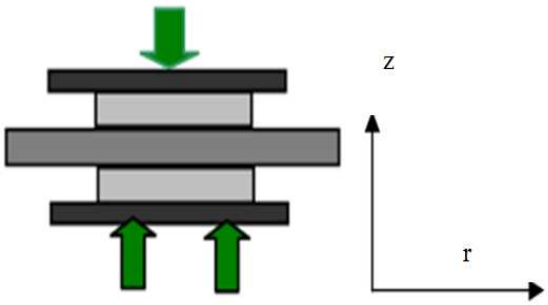

Figure 3.10 Axial compressive stresses

3.2.3.3 Radial Constraints

This is displacement boundary condition (fixed boundaries where the displacements are to be zero) which is applied at the inner radius of the rotor to prevent radial movement of the rotor. At the same time the external radius of the disc is free from stress, as well as displacement constraint (figure 3.15).

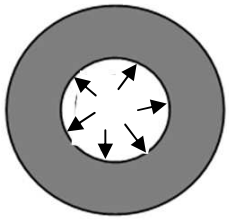

Figure 3.11 Radial Displacement Constraints

3.3 Analytical Analysis Methods in Disk Brake Temperature Distribution

To investigate the thermal stress behavior of brake discs under thermal load, it is necessary to obtain typical temperature distributions in this brake rotor as a function of time. Therefore, the objective of this section is to predict the temperature response of the brake disc design.

As it is shown in figure 3.8 below, disk is like an annulus and pad is like a partial annulus. The brake system clamps the pads through the caliper assembly by brake fluid pressure in the cylinder. Rotary motion of the disk causes the sliding contact between the disk and the pad and generates heat. For calculation of heat generation due to friction, rate of dissipated heat via friction should be taken in to account. This is all to do with the calculation of friction force and the rate of work done by friction force. For the calculation of friction force, the pressure distribution at the contact surfaces of the disk and the pad should be determined.

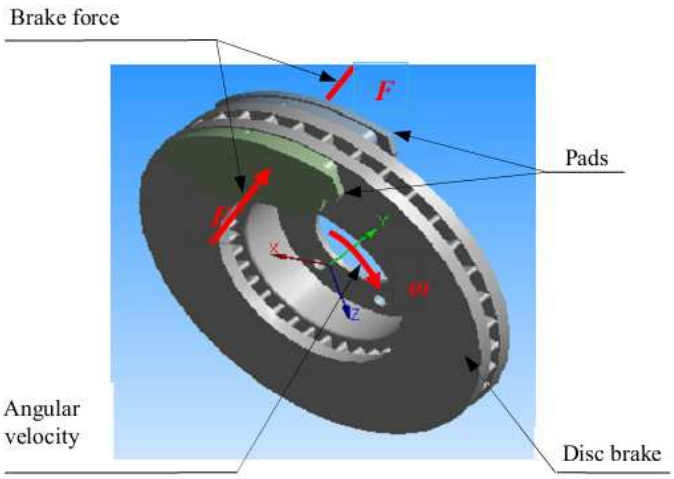

Figure 3.12 Schematic shapes of the disk and the pad in sliding contact

In the contact area of brake components, the pad and the disk, heat is generated due to friction. For calculation of heat generation at the interface of these two sliding bodies, two methods are suggested, macroscopic model and microscopic model.

In case of macroscopic model analysis, brakes are essentially a mechanism to change the energy types. When a car is moving with speed, it has kinetic energy. Applying the brakes, the pads that press against the brake rotor convert this energy into thermal energy. The cooling of brakes dissipates the heat and the vehicle slows down. This is all to do with the first law of thermodynamics, known as laws of conservation of energy which states that energy cannot be created nor destroyed; it can only be converted from one form to another. In the case of brakes, it is converted from kinetic energy to thermal energy.

$$E_c = \frac{1}{2} M V_o^2 \quad \text{.....3.14}$$

Where M is total mass of the vehicle and V_o is the initial speed of the vehicle. To obtain the amount of heat dissipated by each of the disk will be

$$Q = 0.25 m V_o^2 \quad \text{.....3.15}$$

Where, m is the amount of the distributed mass on the front axle of the vehicle. In addition air drags force, total mass of the rotating parts, and inclination of the roads are required.

The second method is Microscopic model. In this case, rate of generated heat due to friction is equal to the friction power. Some of this frictional heat is absorbed by the disk and the rest is absorbed by the pads. If it is supposed that the whole friction power is transferred to the heat energy and heat partition coefficient is stated by parameter γ. For this particular thesis the input data for analysis is taken from roller testing, which results application of microscopic model in this thesis.

3.3.1 Heat Partition Coefficient and Energy Input

The thermal energy generated at the brake friction Interface can be transferred to both the brake rotor and the pads. This partitioning of the thermal energy is dependent on the relative thermal resistances of the pad and brake rotor that are functions of their respective material densities, heat capacities and thermal conductivities as well as of the presence of any transfer film or third body layer at the rubbing interface. Theoretically, the pad thermal resistance should be higher than the rotor thermal resistance in order to protect the brake fluid from high temperatures but the value of the thermal resistance varies from one pad material to another. For the present analysis, the partitioning coefficient (γ) for thermal input to the brake disc was calculated as follows. The thermal effusivity ξ, is given by the following equation:

$$\xi_d = \sqrt{k_d \rho_d c_d} \quad \text{.....3.16a}$$

$$\xi_p = \sqrt{k_p \rho_p c_p} \quad \text{.....3.16b}$$

$$S_p = \varphi_0 \int_{r_2}^{r_3} r\,dr = \frac{\varphi_0}{2}(R_p^2 - r_p^2) = \frac{65\text{deg}}{2} * \left((0.12)^2 - (0.06)^2\right) = 0.0061236\text{m}^2 \quad \text{.....3.16c}$$

$$S_d = 2\pi \int_{r_2}^{r_3} r\,dr = \pi(R_d^2 - r_d^2) = \pi\left((0.12)^2 - (0.06)^2\right) = 0.033912\text{m}^2 \quad \text{.....3.16d}$$

Using values of table 3.3 for k_d, c_d, k_p, c_p, and table 3.2 for values of ρ_d and ρ_p, we will get values of thermal effusivities of the pad and the disc from equation 3.16a and 3.16b as ξ_d=13787.50 and ξ_p=2645.75. S_p and S_d are frictional contact surfaces of the pad and the disc, respectively. The total heat generated on the frictional contact interface q equals the heat flux into the disk q_d,

and heat flux into the pad q_p. The relative braking energy γ which is called heat partition coefficient is given by the following equation:

$$\gamma = \frac{\xi_d S_d}{\xi_d S_d + \xi_p S_p} = \frac{13787.50 * 0.033912}{(13787.50 * 0.033912) + (2645.75 * 0.0061236)} = \frac{490}{490 + 16.2} = 0.96.....3.17$$

Where ξ_p and ξ_d are thermal effusivities of the pad and the disc, and the This partitioning of the thermal energy is dependent on the relative thermal resistances of the pad and brake rotor that are functions of their respective materials densities, heat capacities and thermal conductivities as well as of the presence of any transfer film or third body layer at the rubbing interface.

The heat flux generated by pressing the pad against the rubbing surface of the rotor is the only source of heat input to the model. The magnitude of this heat flux can be calculated from basic energy considerations. Energy input is a function of speed, coefficient of friction, radius of rotor, and pressure distribution.

In a braking system, the mechanical energy is transformed into a calorific energy. This energy is characterized by a total heating of the disc and pads during the braking phase. The heat quantity in the contact area is the result of plastic micro deformations generated by the friction forces. To obtain heat flux at the surfaces of two components of the brake system, we divide rate of thermal energy by the surface contact area of each component. Energy input is of two types: uniform pressure and uniform wear.

Contac surface element of the disc and the pad is shown on the figure 3.9. When disc slides over the pad, heat is generated at the interface due to friction and this heat is partitioned between the two bodies. The thermal energy generated at the brake friction interface can be transferred to both the brake rotor and the pads. The partitioning of heat is a function of the thermal properties of the bodies, the contact geometry and the sliding speed [23]. The rate of heat generated due to friction between these surfaces is calculated as follows:

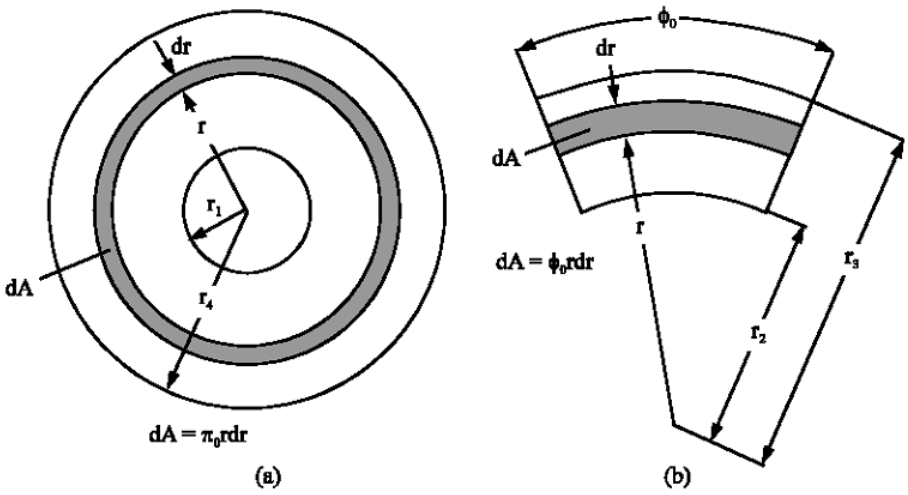

Figure 3.13 Contac surface elements of two components a) the disc and b) the pad.

$$d\dot{E} = dP = VdF_f = r\omega\mu p\varphi_o rdr \quad \text{..3.11a}$$

$$d\dot{E} = d\dot{E}_p + d\dot{E}_d \quad \text{.....3.18b}$$

$$d\dot{E}_p = (1-\gamma)dP = (1-\gamma)\omega\mu p\varphi_0 r^2 dr \quad \text{.....3.18c}$$

$$d\dot{E}_d = \gamma dP = \gamma\omega\mu p\varphi_0 r^2 dr \quad \text{.....3.18d}$$

Where,

$d\dot{E}$ is the rate of heat generated due to friction between two sliding components

V is the relative sliding velocity and

dF_f is the friction force.

The terms dE_p and dE_d are the amount of absorbed heat by the pad and the disk, respectively.

Therefore, to calculate the frictional heat generation at the contact surfaces of two components of the brake system, parameters, e.g. the friction coefficient between two sliding components, relative sliding velocity, geometry of the disk brake rotor and the pad, and the pressure distribution at the sliding surfaces must be available. There are two types of pressure distribution: uniform pressure and uniform wear pressure distribution

In uniform pressure $(p = p_{max})$ heat flux q on a contact area is updated per the pressure distribution at every simulation step. Heat flux for uniform pressure is a function of time and space variable r; the angular velocity decreases with time during braking action and the work done by friction force grows as radial space variable increases. This phenomenon is quite often when the pads are new. Heat flux in the pad is given below.

$$q_p(r,t) = \frac{d\dot{E}_p}{dS_p} = \frac{(1-\gamma)\omega\mu p\varphi_0 r^2 dr}{\varphi_0 r dr} = (1-\gamma)\mu pr\omega(t) \quad \text{.....3.19a}$$

$$q_{0p}(r) = q_{01}(r,0) = \frac{d\dot{E}_p}{dS_p} = \frac{(1-\gamma)\omega\mu p\varphi_0 r^2 dr}{\varphi_0 r dr} = (1-\gamma)\mu pr\omega_o \quad \text{.....3.19b}$$

Similarly Heat flux in the disc is given below

$$q_d(r,t) = \frac{d\dot{E}_d}{dS_d} = \frac{\gamma\omega\mu p\varphi_0 r^2 dr}{2\pi r dr} = \frac{\varphi_0}{2\pi}\gamma\mu pr\omega(t) \quad \text{.....3.19c}$$

$$q_{0d}(r) = \frac{d\dot{E}_d}{dS_d} = \frac{\gamma\omega\mu p\varphi_0 r^2 dr}{2\pi r dr} = \frac{\varphi_0}{2\pi}\gamma\mu pr\omega_o \quad \text{.....3.19d}$$

Where $dS_{d,p}$ is a surface contact area of disc and pads respectively.

In uniform wear ($P = P_{max} r_p/r$) however, assumption of uniform wear is more realistic after several braking application. This thesis focuses on uniform wear pressure distribution. Heat flux obtained for the uniform wear is just a function of time and it is independent of the space variable; the work done by friction force is the same at radial direction. This fact is seen by in pads as follows.

By inserting $P = P_{max} r_p/r$ in equation 3.19a, we will have

$$q_p(t) = (1-\gamma)\mu p_{max} r_p \omega_o \left(1 - \frac{t}{t_b}\right) \quad \text{.....3.20a}$$

And heat flux in the disc is obtained by inserting $P = P_{max} r_p/r$ in equation 3.19d, we will have

$$q_d(r,t) = q_{0d}(r) * (1 - \frac{t}{t_b}) = \frac{\varphi_0}{2\pi} \gamma \mu p_{max} r_d \omega_o . * (1 - \frac{t}{t_b}) \text{.....3.20b}$$

q_{op}, q_{od} is initial heat fluxes for pads and disc

γ - is the heat partitioning factor,

φ_0 - is the cover angle of pad,

μ - is the friction coefficient,

ω - is the angular velocity,

r - is the radial coordinate,

z - is the axial coordinate,

r_p and R_p - are the internal and external radius of the pad.

The heat flux rate defined in Equations above is a function of vehicle speed but was otherwise assumed to apply uniformly over both rubbing surfaces of the disc. In reality, the generated heat flux in a disc brake is non-uniform and time-dependent over the rubbing surface. This thesis focuses on uniform wear of heat flux distributions at t=0. These assumptions were made in order to simplify the thermal analysis which was only intended to predict typical temperature distributions for input to the thermal stress analysis. From equations 3.19d and 3.19b, Table 3.2 (for coefficient of friction), and 1Mpa pressure (from specification),

$$q_d(t) = \frac{65^o}{2\pi} * 0.91 * 0.35 * 1 * 10^6 * 0.0635 * 300 * (1 - \frac{t}{t_b})$$

$$q_d(t) = 626321.68 * (1 - \frac{t}{4.5}) \sim 626{,}321.68 \text{.....3.20c}$$

$$q_p(t) = (1-\gamma)\mu p V_o (1 - \frac{t}{t_b}) = 0.09 * 0.35 * 1 * 10^6 * 0.0635 * 300 * (1 - \frac{t}{t_b})$$

$$q_p(t) = 342900 * (1 - \frac{t}{4.5}) \sim 342900 \text{ .....3.20d}$$

Taking these values, the difference between heat flux shared between disc and pad is shown graphically as in figure 3.10 below.

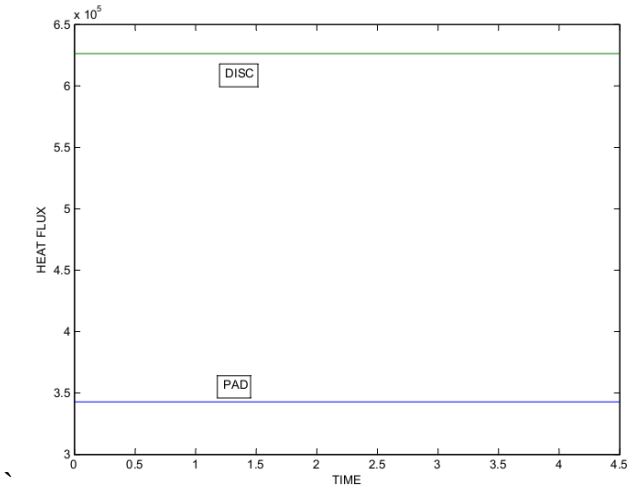

Figure 3.14 Heat Flux Distributions between disc and pad

3.3.2 Differential Equation of Heat Conduction

The basic law that gives the relationship between the heat flow and the temperature gradient, based on experimental observations, is generally named after the French mathematical- physicist Joseph- Fourier [24], who used it in his analytic theory of heat. For a homogeneous, isotropic solid (i.e., material in which thermal conductivity is independent of direction) the Fourier law is given in the form.

$$q(r,t) = -k\nabla T(z,t) \qquad \text{…….3.21}$$

Where the temperature gradient is a vector normal to the isothermal surface, the heat flux rector q(z, t) represents heat flow per unit time, per unit area of the isothermal surface in the direction of the decreasing temperature, and k is called the thermal conductivity of the material which is a positive, scalar quantity. Since the heat flux vector q(z, t) points in the direction of decreasing temperature, the minus sign is included in equation 3.21 to make the heat flow a positive quantity

We now derive the differential equation of heat conduction for a stationary, homogeneous, isotropic solid with heat generation within the body (figure 3.11). Heat generation may be due to nuclear, electrical, chemical, x-ray, or other sources that may be a function of time and/or

position. The heat generation rate in the medium, generally specified as heat generation per unit time, per unit volume, is denoted by the symbol g(z,t), and if SI units are used, is given in the units W/m^3.

We consider the energy-balance equation for a small control volume V, illustrated in figure 3.11, stated as

$$\begin{bmatrix}\text{rate of heat entering through}\\ \text{the bounding surfaces of V}\end{bmatrix}+\begin{bmatrix}\text{rate of energy}\\ \text{generation in V}\end{bmatrix}=\begin{bmatrix}\text{rate of energy}\\ \text{generation in V}\end{bmatrix} \quad \text{……3.22a}$$

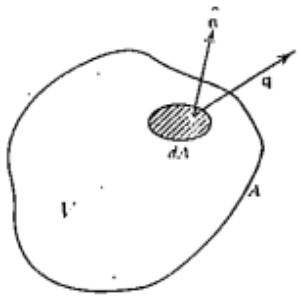

Figure 3.15 Nomenclature for the derivation of heat conduction equation.

Various terms in this equation are evaluated as

$$\begin{bmatrix}\text{rate of heat entering through}\\ \text{the bounding surfaces of V}\end{bmatrix}=-\int_A q.ndA=-\int_V \nabla.qdV \quad \text{……...…….3.22b}$$

where A is the surface area of the volume element V, ft is the outward-drawn normal unit vector to the surface element dA, q is the heat flux vector at dA; here, the minus sign is included to ensure that the heat flow is into the volume element V, and the divergence theorem is used to convert the surface integral to volume integral. The remaining two terms are evaluated as

$$\begin{bmatrix}\text{rate of energy}\\ \text{generation in V}\end{bmatrix}=\int_V g(z,t)dV \quad \text{…….3.22c}$$

$$\begin{bmatrix}\text{rate of energy}\\ \text{generation in V}\end{bmatrix}=\int_V \rho C_p \frac{\partial T(z,t)}{\partial t}dV \quad \text{……...….3.22d}$$

The substitution of equations (3.22b, c, d) into equation 3.22a yields

$$\int_V \left[-\nabla.q(z,t) + g(z,t) - \rho C_p \frac{\partial T(z,t)}{\partial t} \right] dV - 0 \qquad \text{.....3.22e}$$

Equation 3.22e is derived for an arbitrary small-volume element V within the solid; hence the volume V may be chosen so small as to remove the integral. We obtain

$$-\nabla.q(z,t) + g(z,t) = \rho C_p \frac{\partial T(z,t)}{\partial t} \qquad \text{.....3.23}$$

Substituting q(z, t) from equation 3.21 into equation 3.23, we obtain the differential equation of heat conduction for a stationary, homogeneous, isotropic solid with heat generation within the body as

$$-\nabla.[k\nabla T(z,t)] + g(z,t) = \rho C_p \frac{\partial T(z,t)}{\partial t} \qquad \text{.....3.24}$$

For a medium with constant thermal conductivity and no heat generation, equations 3.24 become the diffusion or the Fourier equation

$$\nabla^2 T(z,t) = \frac{1}{\alpha} \frac{\partial T(z,t)}{\partial t} \qquad \text{..... 3.25}$$

Where, $\alpha = \dfrac{k}{\rho C_p}$ is thermal diffusivity

Here, the thermal diffusivity α is the property of the medium and has a dimension of square length per time. The physical significance of thermal diffusivity is associated with the speed of propagation of heat into the solid during changes of temperature with time. The higher the thermal diffusivity, the laster is the propagation of heat in the medium.

In the cylindrical coordinate system equations 3.25, become

$$\frac{\partial^2 T}{\partial r^2} + \frac{1}{r}\frac{\partial T}{\partial r} + \frac{1}{r^2}\frac{\partial^2 T}{\partial \theta^2} + \frac{\partial^2 T}{\partial z^2} = \frac{1}{\alpha}\frac{\partial T}{\partial t} \qquad \text{.....3.26}$$

To evaluate the contact temperature conditions, analytical techniques have been developed. The starting point for the analysis of the temperature field in the disc volume is the parabolic heat

conduction equation in the cylindrical coordinate system (r, θ, z) which is centered in the axis of disc and z points to its thickness [22]

By looking at the mechanism of the disk brake, it may be deduced that we have temperature gradient in θ direction.The distribution of heat flow will be uniform in circumferential direction, which means that neither temperature nor heat flow will vary in θ direction nor thus, the heat conduction equation for the disk and the pad will be a function of r, z and t while independent of θ [25].

$$\frac{\partial^2 T}{\partial r^2}+\frac{1}{r}\frac{\partial T}{\partial r}+\frac{\partial^2 T}{\partial z^2}=\frac{1}{\alpha}\frac{\partial T}{\partial t} \quad \text{.....3.27a}$$

Again for this thesis temperature distribution varies only along disc thickness. Variation of temperature along radius is canceled due to constant heat flux applied on disc surface. Therefore equation above is reduced to the following equation

$$\frac{\partial^2 T}{\partial z^2}=\frac{1}{\alpha}\frac{\partial T}{\partial t} \quad \text{.....3.27b}$$

The method of splitting the solution for T in to two parts, i.e., T=w+s, is sometimes known as 'partial solutions'. The goal in using this method is to transform a problem that cannot, directly, be solved with separation of variables into a problem (or problems) that can [26]. The partial solutions technique is one example of a general method known as superposition, in which two or more solutions to a modified problem are superimposed (or, equivalently, added) to form a solution to the whole problem (differential equation, boundary conditions, and initial conditions) under consideration. The feature of the differential equation and boundary conditions that allows for this method is linearity for which a sum of independent solutions to the DE will also be a solution.

The partial solutions method, which is shown in this section, relies on the splitting of the sought T solution into a steady state part and a transient part. The transient part will conform to the separation of variables requirements. We consider temperature distribution only along thickness of the disc. For a condition in which surface of the disc at z=0 is insulated, initially at T_0, and surface at z=δ/2 heat flux of magnitude q_o as follows

Differential equation $$\frac{\partial T^2}{\partial z^2} = \frac{1}{\alpha_d}\frac{\partial T}{\partial t} \quad \text{.....3.28a}$$

Boundary and initial conditions: $$\begin{cases} \dfrac{\partial T(0,t)}{\partial z} = 0 \\ -k\dfrac{\partial T(z,t)}{\partial z} = q_o \\ T(x,0) = T_i \end{cases} \quad \text{.....3.28b}$$

where the property $\alpha=k/\rho c_p$ is the thermal diffusivity of the material.

The dimensionless parameter of partial differential equation given in Equation 3.28a together with its boundary and initial conditions can be solved using several analytical and numerical techniques, including the Laplace or other transform methods, the method of separation of variables, the finite difference method, and the finite-element method. Here we use the method of separation of variables developed by J. Fourier [24] and is based on expanding an arbitrary function (including a constant) in terms of Fourier series. The method is applied by assuming the dependent variable to be a product of a number of functions, each being a function of a single independent variable. This reduces the partial differential equation to a system of ordinary differential equations, each being a function of a single independent variable. We now attempt to nondimensionalize the problem (equation 3.28a) by defining dimensionless space variables. These are convenient choices since both θ and Z vary between 0 and 1. We do the analysis by taking the thickness of the disc as z axis.

$$\theta = \frac{(T - T_i)k}{q_o\delta}, \quad Z = \frac{z}{\delta}, \quad \tau = \frac{\alpha}{\delta^2}t \quad \text{.....3.29}$$

Then, the problem statement become as follows in equation 3.29. Because the wall receives a flux at Z= 1, yet is insulated at Z= 0, it will never attain an equilibrium state. Rather, the temperature throughout the wall will continuously increase with time.

$$\frac{\partial\theta}{\partial\tau}=\frac{\partial\theta^2}{\partial Z^2} \quad \text{.....3.30a}$$

$$\left.\frac{\partial\theta}{\partial Z}\right|_{Z=0}=0 \quad \text{.....3.30b}$$

$$\left.\frac{\partial\theta}{\partial Z}\right|_{Z=1}=1 \quad \text{.....3.30c}$$

$$\theta(Z,\tau=0)=0 \quad \text{.....3.30d}$$

The analytical procedure follows the general approach developed by a superposition of partial solutions

$$\theta(Z,\tau)=w(Z,\tau)+s(Z)+\theta_m(\tau) \quad \text{.....3.31}$$

The function $w(Z,\tau)$ is a transient part which decays to 0 for large t, $\theta_m(\tau)$ is the mean (or average) temperature in the wall which will be a function solely of time, and s(x) can be interpreted as a stationary solution; it is the temperature profile in the wall which occurs after the transient portion has decayed. Alternatively s(x) represents the solution to $\theta(Z,\tau)$-$\theta_m(\tau)$ for τ approaches infinity. This approach therefore makes the assumption that, for adequately long times past the initial transient, the time and position dependencies on temperature are additive. Such an approach will be valid because the boundary conditions are not functions of time.

The solution for the mean temperature $\theta_m(\tau)$ is obtained by integration of Eq. (3.30a), over Z from 0 to 1;

$$\int_0^1\frac{\partial\theta}{\partial\tau}dZ=\int_0^1\frac{\partial\theta^2}{\partial Z^2}dZ$$

$$\frac{d}{\partial\tau}\int_0^1\theta dZ=\left.\frac{d\theta}{dZ}\right|_1-\left.\frac{d\theta}{dZ}\right|_0 \qquad \text{and} \qquad \int_0^1\theta dZ=\theta_m$$

$$\int_0^1\theta dZ=T_m,\quad \left.\frac{d\theta}{dZ}\right|_1=1 \quad \left.\frac{d\theta}{dZ}\right|_0=0$$

$$\Rightarrow\frac{d\theta_m}{\partial\tau}=1 \quad \text{.....3.32}$$

Since the mean temperature is zero at $\tau = 0$, solution of the above differential equation gives the result $\theta_m(\tau) = \tau$ .This could have been anticipated: the rate change in mean temperature will be proportional to the rate of heat addition to the wall. Since the latter is a constant and equal to unity, the mean temperature will be equal to τ. Now replace Eq. (3.31) into the problem statement for θ;

$$\frac{\partial w(Z,\tau)}{\partial \tau} + \frac{\partial \theta_m(\tau)}{\partial \tau} = \frac{\partial^2 w(Z,\tau)}{\partial Z^2} + s''(Z) \quad \text{.....3.33a}$$

$$\left.\frac{\partial w}{\partial Z}\right|_0 + s'(0) = 0 \quad \text{.....3.33b}$$

$$\left.\frac{\partial w}{\partial Z}\right|_1 + s'(1) = 1 \quad \text{.....3.33c}$$

$$w(Z,0) + s(Z) + \theta_m(0) = 0 \quad \text{.....3.33d}$$

The associated problem for s(Z) represents the steady state solution to $\theta(Z,\tau) - \theta_m(\tau)$, and is

$$s'' = 1, \quad s'(0) = 0, \quad s'(1) = 1$$

This represents, equivalently, a uniform heat sink of unit strength in a thickness with a uniform unit flux at one side and adiabatic conditions at the other. The net heat addition to the disc is zero (the sink balances the input flux), and a steady condition is physically realizable. The solution for s is

$$s(Z) = \frac{Z^2}{2} + C \quad \text{.....3.34}$$

Where C is an undetermined constant, this arises because both boundary conditions for s are in terms of derivatives of s the solution to s can therefore be shifted by an arbitrary constant. The constant, however, can be pinned down by invoking the definition of the average temperature; the integral of θ over Z is defined as θ_m and this implies (using $\theta = \theta_m + s$ for $t \rightarrow \infty$) that the integral of s over Z must be zero. Consequently, $C = -1/6$.

The problem for w is

$$\frac{\partial w}{\partial \tau} = \frac{\partial^2 w}{\partial Z^2} \quad \text{.....3.35a}$$

$$\left.\frac{\partial w}{\partial Z}\right|_0 = 0 \quad \text{.....3.35b}$$

$$\left.\frac{\partial w}{\partial Z}\right|_1 = 0 \quad \text{.....3.35c}$$

$$w(Z,0) = -s(Z) \quad \text{.....3.35d}$$

This has the general solution,

$$w = \sum_{n=1} A_n \varphi_n(Z) e^{-\lambda_n^2 \tau} \quad \text{.....3.36}$$

The eigenfunctions and eigen conditions to the solution are

$$\varphi_n(Z) = \cos(\lambda_n Z), \qquad \lambda_n = n\pi \quad n = 1,2.3,...$$

The expansion coefficients are determined following the procedures established below;

$$\begin{aligned} A_n &= -2\int_0^1 s(Z)\varphi_n(Z)dz \\ &= \frac{2}{\lambda_n}\int_0^1 s(Z)\varphi_n''(Z)dz \\ &= \frac{2}{\lambda_n}\left[s(Z)\varphi_n'(Z)\Big|_0^1 - s'(Z)\varphi_n(Z)\Big|_0^1 - \int_0^1 s''(Z)\varphi_n(Z)dz \right] \\ &= \frac{2(-1)^n}{\lambda_n^2} \end{aligned}$$

And the complete solution for the temperature distribution is

$$\theta = -\frac{1}{6} + \tau + \frac{Z^2}{2} - 2\sum_{n=1} \frac{(-1)^n}{\lambda_n^2} \cos(\lambda_n Z) e^{-\lambda_n^2 \tau} \quad \text{.....3.37a}$$

Substituting equation 3.29 in equation 3.37a above gives

$$T(z,t) = T_i + \frac{q_o \delta}{k}\left[-\frac{1}{6} + \frac{\alpha}{\delta^2} t + \frac{z^2}{2\delta^2} - 2\sum_{n=1} \frac{(-1)^n}{\lambda_n^2} \cos\left(\lambda_n \frac{z}{\delta}\right) e^{-\lambda_n^2 \left(\frac{\alpha}{\delta^2}\right) t} \right] \quad \text{.....3.37b}$$

$$\Delta T(z,t)=\frac{q_o\delta}{k}\left[-\frac{1}{6}+\frac{\alpha}{\delta^2}t+\frac{z^2}{2\delta^2}-2\sum_{n=1}\frac{(-1)^n}{\lambda_n^2}\cos\left(\lambda_n\frac{z}{\delta}\right)e^{-\lambda_n^2\left(\frac{\alpha}{\delta^2}\right)t}\right]\text{.....3.37c}$$

If transient temperature on surface of the disc is required, simply z=δ is inserted in equation above.

$$T(t)=T_i+\frac{q_o\delta}{k}\left[-\frac{1}{6}+\frac{\alpha}{\delta^2}t+\frac{1}{2}-2\sum_{n=1}\frac{(-1)^n}{\lambda_n^2}\cos(\lambda_n)e^{-\lambda_n^2\left(\frac{\alpha}{\delta^2}\right)t}\right]\text{.....3.37d}$$

$$\Delta T(t)=\frac{q_o\delta}{k}\left[-\frac{1}{6}+\frac{\alpha}{\delta^2}t+\frac{1}{2}-2\sum_{n=1}\frac{(-1)^n}{\lambda_n^2}\cos(\lambda_n)e^{-\lambda_n^2\left(\frac{\alpha}{\delta^2}\right)t}\right]\text{.....3.37e}$$

3.4 Methods of Analyzing Disc Stress Components

We consider that the disc is made of a homogeneous isotropic material. The disc is assumed as sandwiched between the two pads, in which temperature variation occurs only along thickness of the disc. Analytical solution for thermal stress components during thermal transients will be done only for areas where exposed to high temperature variation during brake application, this specifically include surface of the rotor closest to the pads. Due to symmetry only cross section of the thickness and circumferential slice of the rotor is used for analytical reasoning. It is assumed that the thermomechanical properties do not change during a thermal transient and that the strain rates due to the thermal loading are small, so both the inertia and thermo mechanical coupling terms in the thermoelasticity governing equations can be neglected.

By taking the above boundary conditions as an input, we can drive thermal stress by using stress-strain equation 3.11b and 3.11c. Free thermal expansion of an element of a plate along circumferential and axial will be completely suppressed by applying stress σ_z and σ_θ respectively. By putting ε_z =0, σ_r =0 and ε_θ =0 in stress-strain equation of 3.11b and 3.11c, we will get [27] the following equation

$$\sigma_{zz} = \sigma_{\theta\theta} = -\frac{\alpha E \Delta T}{1-v} \quad \text{.....3.38}$$

By combining with thermal equation 3.37e we will get transient stress as a function of disc thickness as follows

$$\sigma_{zz} = \sigma_{\theta\theta} = -\frac{\alpha E}{1-v}\frac{q_o \delta}{k}\left[-\frac{1}{6} + \frac{\alpha}{\delta^2}t + \frac{z^2}{2\delta^2} - 2\sum_{n=1}\frac{(-1)^n}{\lambda_n^2}\cos\left(\lambda_n \frac{z}{\delta}\right)e^{-\lambda_n^2\left(\frac{\alpha}{\delta^2}\right)t}\right] \quad \text{.....3.39a}$$

Equation above is true as far as temperature variation occurs along perpendicular direction to z and θ direction. But, in equation 3.39a σ_{zz} is parallel with direction of temperature expansion, and $\sigma_{\theta\theta}$ i.e. perpendicular to direction of temperature expansion. Which means equation 3.39a is used only for $\sigma_{\theta\theta}$.

$$\sigma_{\theta\theta} = -\frac{\alpha E}{1-v}\frac{q_o \delta}{k}\left[-\frac{1}{6} + \frac{\alpha}{\delta^2}t + \frac{z^2}{2\delta^2} - 2\sum_{n=1}\frac{(-1)^n}{\lambda_n^2}\cos\left(\lambda_n \frac{z}{\delta}\right)e^{-\lambda_n^2\left(\frac{\alpha}{\delta^2}\right)t}\right] \quad \text{.....3.39b}$$

σ_{zz} is uniform axial stress through the thickness and its variation is negligible through thickness. Therefore we can take temperature difference between the two surfaces to calculate axial stress. Temperature at this point is approximated as temperature difference because temperature at the surface is very high and temperature at the lower surface is very low so that this temperature variation is used to calculate uniform compressive axial stress which is constant value at specified time. As a result equation 3.38 is modified as follows.

$$\sigma_{zz} = -\frac{\alpha E}{1-v}\left(T_1(t) - T_2(t)\right) \quad \text{.....3.39c}$$

Where T_1 and T_2 temperature at two different surface

External radius of the disc is free from the stress. The thermal stress in the disc free from external force is obtained by superposing on the stress in equation 3.38 the stress due to application of equal and opposite distribution of force on the edges. This stress is the stress produced in the disc by tensile force of intensity αTE distributed at the ends. This force has the following resultant

$$\int_0^{\delta} \alpha E \Delta T dz \quad \text{……..…….3.40a}$$

And at sufficient distant from the end they will produce approximately uniformly distributed radial tensile stress of magnitude

$$\frac{1}{\delta(1-v)}\int_0^{\delta} \alpha E \Delta T dz \quad \text{……...……3.40b}$$

So that the radial thermal stress in the disc with the free ends at the considerable distance from the end will be obtained by inserting equation3.40a in compressive radial stress as follows.

$$\sigma_{rr} = -\frac{\alpha E \Delta T}{1-v} + \frac{1}{\delta(1-v)}\int_0^{\delta} \alpha E \Delta T dz \quad \text{…….……..……..3.41a}$$

Combining with thermal equation of 3.37e we will get radial stress distribution through thickness of the disc as follows.

$$\sigma_{rr} = -\frac{\alpha E}{1-v}\frac{q_o \delta}{k}\left[-\frac{1}{6} + \frac{\alpha}{\delta^2}t + \frac{z^2}{2\delta^2} - 2\sum_{n=1}\frac{(-1)^n}{\lambda_n^2}\cos\left(\lambda_n \frac{z}{\delta}\right)e^{-\lambda_n^2\left(\frac{\alpha}{\delta^2}\right)t}\right] + \frac{\alpha E q_o \delta}{k\delta(1-v)}\int_0^{\delta}\left[-\frac{1}{6} + \frac{\alpha}{\delta^2}t + \frac{z^2}{2\delta^2} - 2\sum_{n=1}\frac{(-1)^n}{\lambda_n^2}\cos\left(\lambda_n \frac{z}{\delta}\right)e^{-\lambda_n^2\left(\frac{\alpha}{\delta^2}\right)t}\right]dz \quad \text{…….3.41b}$$

If T is even function of z such that the mean value over the thickness of the plate is zero, the resultant force per unit run of edge is zero, and it produces no stress except near the edge. If the mean value of T is not zero, uniform tension in the r and z directions corresponding to the resultant force on the edge must be super posed on the compressive stress of equation 3.38. In addition to this the temperature is not symmetrical with respect to the rz plane; we must add the bending stress. In this manner we finally arrive at the equation below

$$\sigma_{rr} = -\frac{\alpha E T}{1-v} + \frac{1}{\delta(1-v)}\int_0^{\delta} \alpha E T dz + \frac{24z}{2\delta^3(1-v)}\int_0^{\delta} \alpha E T z dz \quad \text{……..3.42}$$

By using equation 3.42 we can easily calculate thermal stress in the in the rotor if distribution of temperature T over the thickness of the rotor is known. And due to symmetry in boundary conditions as well as geometry of the disc brake, there are no shear stress distributions.

3.4.1 Von Mises Theory Analysis and Fatigue Life Time Estimation

In inelastic stress analysis, a mathematical equation involving the three principal normal stresses, known as a yield function, is generated. If the calculated yield function is greater than the yield strength of a material, plastic straining and subsequent strain softening or hardening occurs. Generally, there are several yield functions available to check whether the stress state is beyond the elastic region. These include the von Mises stress criterion, the maximum shear stress criterion and the maximum normal stress criterion. If a material is subjected to stresses beyond the elastic region, change of the yield surface occurs due to the development of plastic strain. There are two basic types of change of the yield surface. One is based on the assumption that the centre of the yield surface remains fixed whilst, at the same time, the yield surface expands without changing shape. This is known as isotropic hardening. The other, known as kinematic hardening, is based on the assumption that the yield surface translates within the stress space but does not change size or shape. Both the maximum shear stress (Tresca) and von Mises stress criteria are widely used to predict the yield surfaces of ductile materials because they have been found to fit the experimental results of ductile materials [28]. In contrast, the maximum normal stress criterion is commonly used to predict fracture for brittle materials because their yield stresses occur at the low strain levels and are difficult to define.

Tresca and von Mises are generally applied when structural material is ductile. The von Mises theory generally predicts failure more accurately, but the Tresca theory is often used in design because it is simpler to apply and is more consecutive.

Von Mises theory relates the distortional energy of a point under a general state of stress to that of the tensile specimen at yielding [29]. A hydrostatic state of stress occurs when all three principal stresses are equal. In this situation, the normal strains on all directions are equal and there is no shear stress due to symmetry as well. Consequently, no distortion of the stressed element occurs. Any deviation from this state will cause distortion. A general state of stress can be considered as the superposition of a pure hydrostatic state.

To evaluate the thermal stresses caused by temperature distributions, the elastic von Mises stress (σ_e) is defined in equation 3.43 below was considered, since this parameter, which combines the three principal stresses, was assumed to determine yield (onset of plastic deformation) in metals:

$$\sigma_e = \frac{1}{\sqrt{2}}\left[(\sigma_r - \sigma_\theta)^2 + (\sigma_\theta - \sigma_z)^2 + (\sigma_z - \sigma_r)^2\right]^{1/2} \quad \text{.....3.43}$$

Where σ_1 σ_2 and σ_3 are principal stresses in a cylindrical axis system. Since the elastic stresses and strains are completely reversible and non cumulative, the brake disc model was investigated for one cycle of the braking and cooling period only.

Even though the Von Mises theory is stated above, the failure analysis of gray cast iron material is given in tensile strength only. Gray iron's compressive strength is typically three to four times more than its tensile strength. The lack of graphite associated volume changes allows for a similar Poisson's ratio to other engineering metals. Poisson's ratio remains constant over a large compressive stress range and increases at higher stress levels.

Relations between the plastic strain amplitude and the number of cycles to fracture were first presented in early 1950 papers by Coffin- Manson [32] were based on empirical low cycle fatigue data. They related plastic strain amplitude ε_p to the fatigue life N on log-log axes. The Manson-Coffin relationship between ε_p and N can be written in the form

$$\varepsilon_p = \varepsilon_f N^c \quad \text{.....3.44}$$

Where ε_f is the fatigue ductility coefficient given by the extrapolation of the Manson- Coffin formula to the first half-cycle and c is the slope of the Manson-Coffin curve fitted to experimental data on log-log plots. It is also of interest to note that experimentally determined σ-N curves may be represented by the equation

$$\sigma_a = \sigma_f N^b \quad \text{.....3.45}$$

In this equation, σ_f is the fatigue strength coefficient given by extrapolation of the σ-N curve to the first half-cycle, and b is the slope of the σ-N curve fitted to experimental data plotted

on log-log scales. The exponent b and c varies from material to material. The corresponding values of σ_f, b, ε_f, and c for grey cast iron GG25 are given in table 3.5.

Many machine and automobile parts are subjected to constant total strain amplitude ε_t, which consists of two parts: ε_p, the plastic strain amplitude, and ε_e, the elastic strain amplitude. The elastic strain amplitude in an axial test specimen is related to the stress amplitude σ_a by Hooke's law

$$\varepsilon_e = \frac{\sigma_a}{E} \quad \text{.....3.46}$$

Then, in terms of the total strain amplitude, the fatigue life relation is obtained by equations 3.44-3.46 as

$$\varepsilon_t = \varepsilon_e + \varepsilon_p = \frac{\sigma_f}{E} N^b + \varepsilon_f N^c \quad \text{.....3.47}$$

Table 3.5 Parameters for estimating fatigue life time for GG25 gray cast iron [17].

σ_f (Mpa)	b	ε_f	c
241	-0.115	0.008	-0.36

Chapter Four: Finite Element Analysis Methods and Conditions

4.1 Gray Cast Iron Material

The same material (grey cast iron) is used both in analytical and finite element method. The detail thermal properties and mechanical properties of grey cast iron is discussed in analytical analysis of section 3.1. Thermal properties of grey cast iron, which are thermal conductivity, specific heat capacity, and thermal expansion coefficient, are used as an input for thermal stress analysis. Again mechanical properties of grey cast iron such as Poisson's ratio and modulus of elasticity are used in stress analysis depending up on temperature distributions. These thermal properties and mechanical properties are taken from table 3.3 and 3.2 respectively.

4.2 Finite Element Method Conditions

3-D model developed for the analysis is given below (figure 4.1). Numerical simulations using the ANSYS finite element software package were performed in this study for a simplified version of a disc brake system which consists of the two main components contributing for thermal structural analysis, the disc and the pads. The dimensions and the parameters used in the thermal stress calculation are recapitulated in Table 3.4.

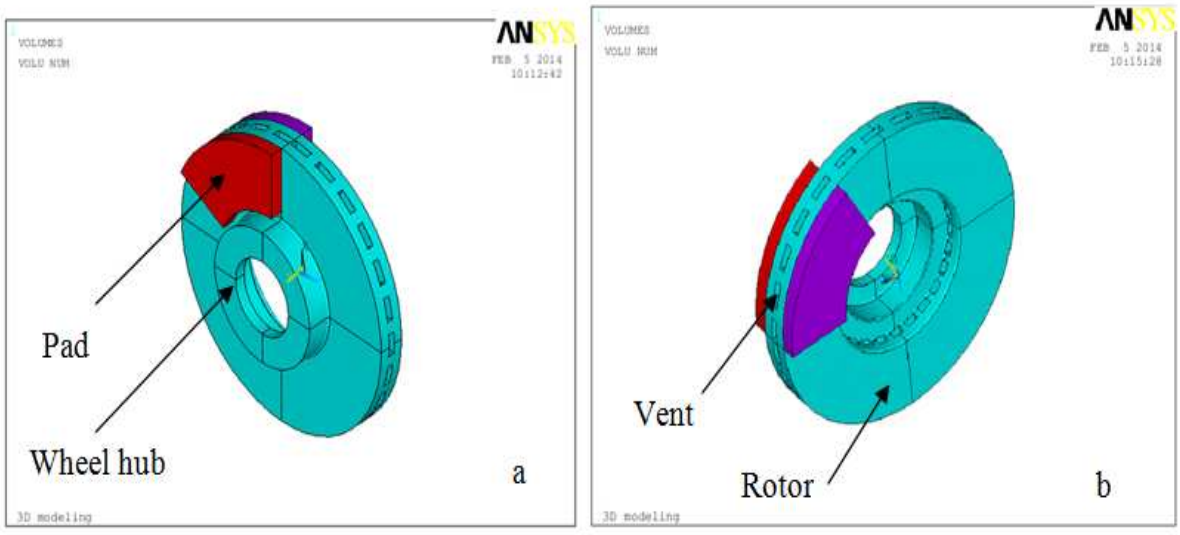

Figure 4.1 3-D modeling of disc and pads with different orientations (a and b)

4.2.1 Using Symmetry Conditions in Modeling Disc Thermal Analysis

In order to accurately conduct the heat transfer and thermal analysis of the vented rotor design chosen for this study, a 3-D model of the brake disc was developed. Since the purpose is to predict typical temperature data for investigating the thermal stress behavior, only the area where the brake disc is subjected to high thermal load was modeled in detail (rotor). The model and analysis of wheel hub is omitted due to the fact that no thermal related problems created in wheel hub, because it is far away from disc pad contact. Furthermore, the rotor was modeled as solid rather than vented rotor [32]. This assumption does not influence the analysis, because temperature and thermal stress are high in this assumption, than in case of vented rotor.

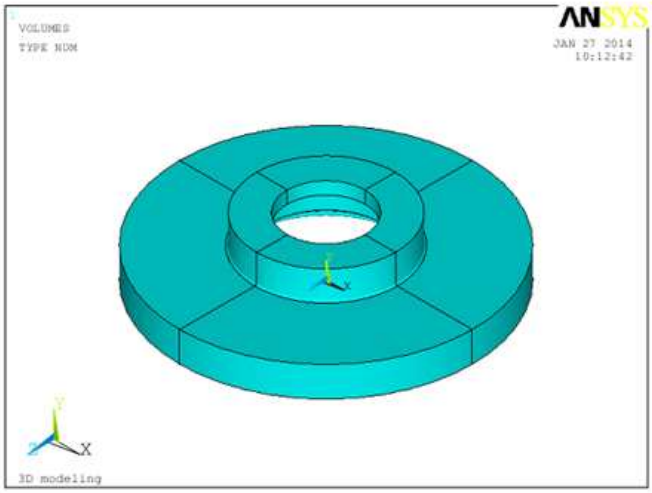

Figure 4.2 3-D modeling of solid rotor assumption

If the physical system under consideration exhibits symmetry in geometry, material properties, and loading, then it is computationally advantageous to model only a representative portion. If the symmetry observations are to be included in the model generation, the physical system must exhibit symmetry in all of the following [31]:

- ✓ Geometry
- ✓ Material properties
- ✓ Loading
- ✓ Degree of freedom constraints

We can use two types of symmetry in modeling disc: axisymmetry (the symmetry about a central axis) and symmetry in material properties and loading.

In axisymmetry, an axisymmetric model is based on the assumption that both the geometry and loading do not vary in the circumferential direction which implies that the measurements (temperature, stress, etc) are also invariant in the circumferential direction. Because the disc is symmetry in circumferential direction, no need of analyzing full disc, just 15.65° segment of the brake disc is selected to analyze structural thermal analysis (figure 4.2). Note that this segment is repeated 23 times to give the complete brake disc.

The second symmetry condition is symmetry in material properties and loading. Once symmetry in geometry is observed, the same symmetry plane or axis should also be valid for the material properties and loading (heat flux, temperature, etc.). As it can be seen in figure 4.1, since the thermal problem in the disk is symmetric in z direction and pads on both direction only the half of the disk with one pad is considered.

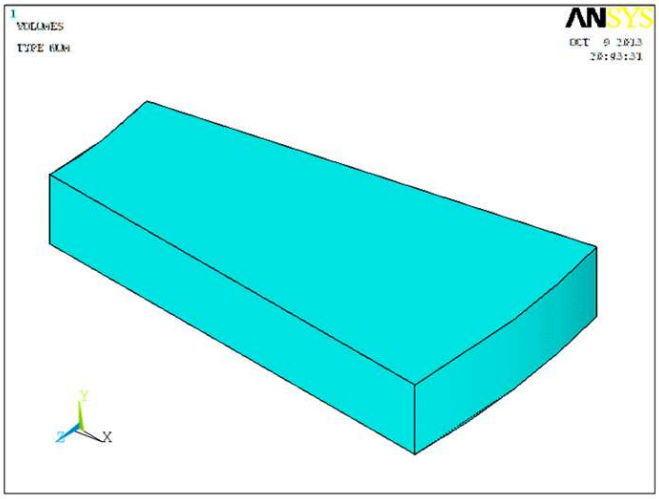

Figure 4.3 Half thickness, 15.65° disc chosen for analysis purpose due to symmetry

4.2.2 Meshing and Loading Conditions the Disc

The elements used for the meshing of the full and ventilated disc are tetrahedral three dimensional elements with 20 nodes (Figure 4.10), both thermally and structurally. In this simulation, the meshing was refined in the contact zone (disc-pad).This is important because in this zone the temperature varies significantly. The disc is meshed using nearly

seven thousand and two hundred 20 noded solid elements with a quadratic interpolation function as shown in Figure 4.3 below.

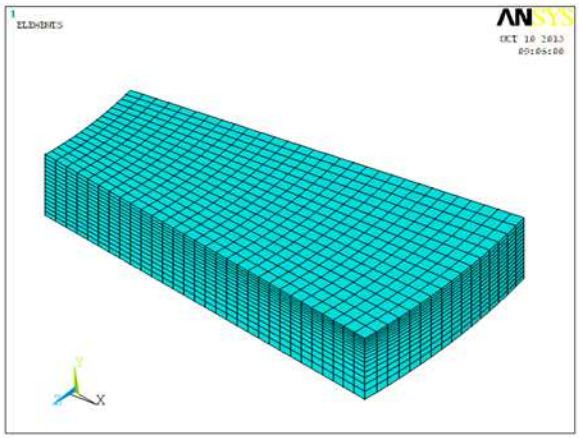

Figure 4.4 Meshing of the disc.

The mesh of the finite elements was selected due to the difference of the obtained peak values of temperature relating to the finest mesh i.e. model with the 16 elements in the circumference and 32433 nodes was used in the thermal analysis. As the mesh should be capable to reproduce the rapid temperature variations in the immediate vicinity of the contact surface, the size of the finite element increased with the distance from the region of generated surface of friction. To avoid inaccurate or unstable results, a proper fixed time step associated with spatial mesh size is essential [30].

The thermal loading is characterized by the heat flux entering the disc through the real contact area (two sides of the disc). We consider heat flux during application of brake (deceleration period) only. Again we consider convection when the car accelerates only. The initial and boundary conditions are introduced into module ANSYS. The thermal calculation will be carried out by choosing the transient state and by introducing physical properties of the materials. The selected data for the numerical application are summarized as follows:

- ✓ Total time of simulation = 4.5 s
- ✓ Increment of time = 0.025s
- ✓ Number of substeps=300
- ✓ Number of load steps=1

4.2.3 Thermal Boundary and Initial Conditions

We assume that the initial temperature of the disc is 30 ^{o}C at t=0 sec. and constant. The heat flux generated by pressing the pad against the rubbing surface of the rotor is the only source of heat input to the model and it is localized in the contact zone of disc-pad in both sides. The magnitude of this heat flux is calculated from basic energy considerations of equation 3.13c in previous chapter, which is 626.321kw/m^2. The cross section of the disc from left and right side is insulated as shown in figure 4.5. Only disc thickness of 12mm is simulated due to symmetry. Internal and external radius of the disk is assumed to be insulated due to their small surface areas.

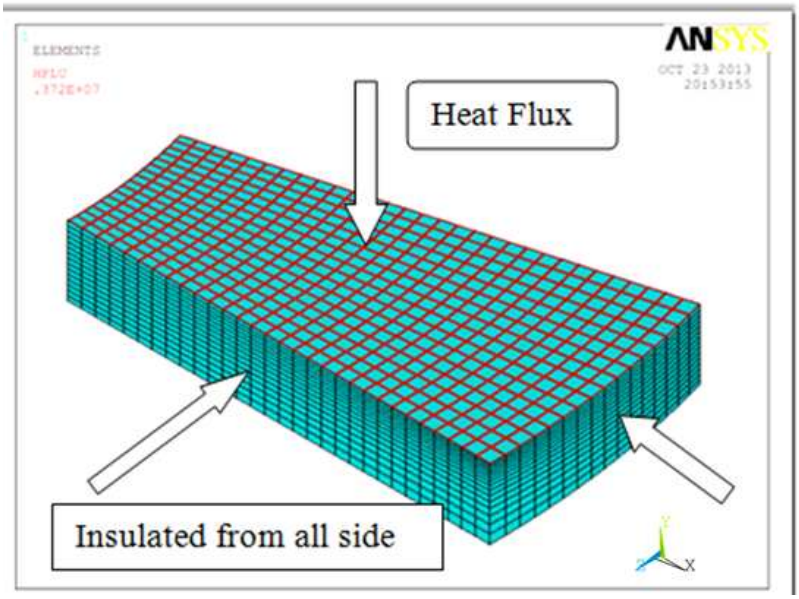

Figure 4.5 Application of heat flux and insulated surfaces

A heat transfer by convection on all the free surfaces of the disc of which the exchange coefficient is h of 60w/m^{2o}C. Heat loss by convection must be defined in the temperature analysis of the brake disc because the vehicle is travelling at high speed and with high rotational velocity of the brake discs, resulting in a high rate of heat transfer by convection. Convection is applied on surface of the disc when the car accelerates (figure 4.5).

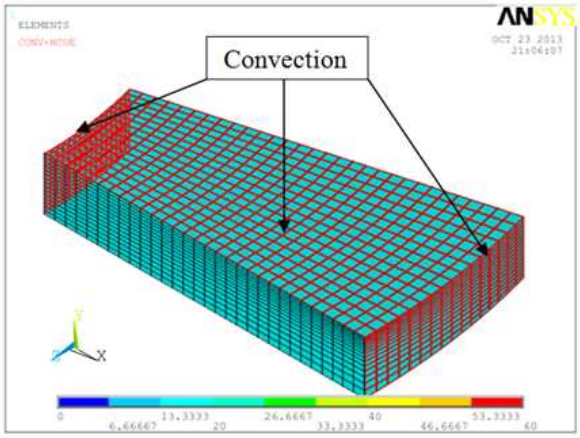

Figure 4.6 Application of convection

4.2.4 Structural Constraints and Boundary Conditions

Circumferential constraints were applied along both radial sections of the brake disc structural model (figure 4.6). In addition, radial and axial constraint was applied to the internal radius and bottom face of the disc respectively as shown in figure 4.7.

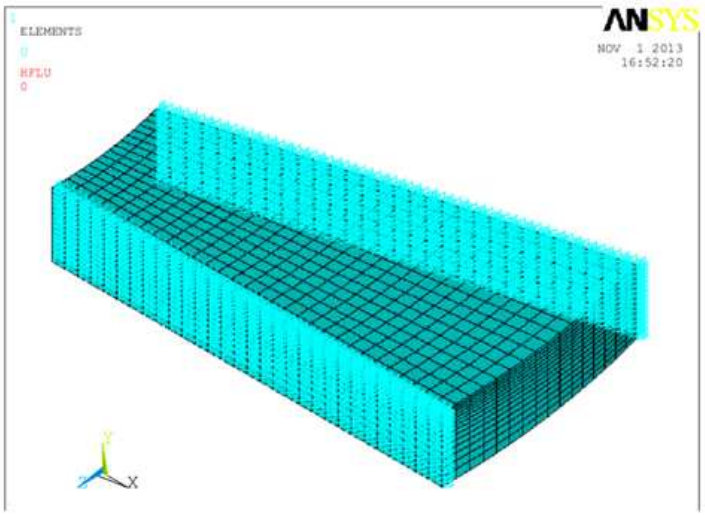

Figure 4.7 Circumferential Constraints

Only thermal stresses were considered because the mechanical loads due to the pad normal pressure, centrifugal force and inertia force are insignificant in comparison [4], Therefore,

it is the non-uniform distribution of temperature that is likely to have the major influence on the deformation of the brake disc.

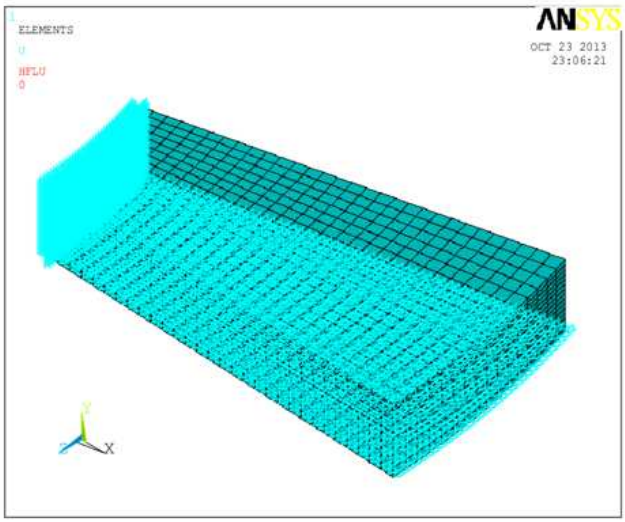

Figure 4.8 Radial constraint at the internal radius, and axial constraint at bottom face

4.3 Methods of Finite Element Analysis

Before the age of computers, analytical methods were used as engineering tools for determining the integrity of a design. For example, Dike [30] illustrated that the mathematical equations for conduction of heat in an isotropic solid could be used to investigate the temperature response of brake disc designs by simplifying complicated parameters such as temperature dependent material properties, real brake disc geometry and complex boundary conditions. However, for real problems involving complex material properties and boundary conditions, a numerical method of analysis is more suitable. The most popular of the various numerical methods that have been developed is the finite element (FE) method. Two types of FE analysis are widely used in brake design: heat transfer analysis to determine transient temperature distributions and thermal stress analysis to determine stresses and strains due to these non-uniform temperature distributions.

Mechanical components in the form of simple bars, beams, etc., can be analyzed quite easily by basic methods of mechanics that provide closed-form solutions. Actual components, however, are rarely so simple, and the designer is forced to less effective approximations of closed-form solutions, experimentation, or numerical methods. There are a great many numerical techniques

used in engineering applications for which the digital computer is very useful. In mechanical design, where computer-aided design (CAD) software is heavily employed, the analysis method that integrates well with CAD is finite-element analysis (FEA). The mathematical theory and applications of the method are vast.

Mechanical component is a continuous elastic structure. FEA divides the structure into small but finite, well-defined, elastic substructures called elements. By using polynomial functions, together with matrix operations, the continuous elastic behavior of each element is developed in terms of the element's material and geometric properties. Loads can be applied within the element, on the surface of the element, or at the nodes of the element. The element's nodes are the fundamental governing entities of the element, as it is the node where the element connects to other elements, where elastic properties of the element are eventually established, where boundary conditions are assigned, and where forces (contact or body) are ultimately applied. A node possesses degrees of freedom. Degrees of freedom are the independent translational and rotational motions that can exist at a node. At most, a node can possess three translational and three rotational degrees of freedom. Once each element within a structure is defined locally in a matrix form, the elements are then globally assembled through their common nodes into an overall system matrix. Applied loads and boundary conditions are then specified and through matrix operations the values of all unknown displacement degrees of freedom are determined. Once this is done, it is a simple matter to use these displacements to determine strains and stresses through the constitutive equations of elasticity.

The establishment of the finite element model and the finite element calculation of this thesis work were conducted through the software package, ANSYS. There are also a number of commercial FEA software packages that are available, such as NASTRAN, Algor, LSDYNA, etc. ANSYS is a combined interactive/batch type computer aided design software package, which contains many mechanical analysis programs developed, commercialized and marked by ANSYS.inc. ANSYS mechanical is a self contained analysis tool incorporating pre-processing such as creation of geometry and meshing, solver and post processing modules in a unified graphical user interface. In addition, it is advanced level of others finite element software. ANSYS is the name commonly used for ANSYS mechanical, general-purpose finite element analysis (FEA) computer aided engineering software tools.

4.3.1 Coupled-Field Analyses and Methods

A coupled-field analysis is a combination of analyses from different engineering disciplines (physics fields) that interact to solve a global engineering problem, hence, we often refer to a coupled-field analysis as a multiphysics analysis. When the input of one field analysis depends on the results from another analysis, the analyses are coupled [31]. The procedure for a coupled-field analysis depends on which fields are being coupled, but two distinct methods can be identified: direct and sequential (load transfer).

The direct method usually involves just one analysis that uses a coupled-field element type containing all necessary degrees of freedom. Coupling is handled by calculating element matrices or element load vectors that contain all necessary terms. An example of a direct method coupled-field analysis is a piezoelectric analysis using the PLANE223, SOLID226, or SOLID227 elements.

The sequential method involves two or more sequential analyses, each belonging to a different field. You couple the two fields by applying results from the first analysis as loads for the second analysis. An example of this is a sequential thermal-stress analysis where nodal temperatures from the thermal analysis are applied as "body force" loads in the subsequent stress analysis. With a physics file-based load transfer, you must explicitly transfer loads using the physics environment. An example of this type of analysis is a sequential thermal-stress analysis where nodal temperatures from the thermal analysis are applied as "body force" loads in the subsequent stress analysis. The physics analysis is based on a single finite element mesh across physics. You create physics files that define the physics environment; these files configure the database and prepare the single mesh for a given physics simulation. The general process is to read in the first physics file and solve. Then read in the next physics field, specify the loads to be transferred, and solve the second physics.

The term sequentially coupled refers to solving one physics simulation after another. Results from one analysis become loads for the next analysis. If the analyses are fully coupled, results of the second analysis will change some input to the first analysis. The complete set of boundary conditions and loads consists of the following:

- ✓ **Base physics loads,** which are not a function of other physics analyses. Such loads also are called nominal boundary conditions.

- ✓ **Coupled loads,** which are results of the other physics simulation.

Typical applications you can solve with ANSYS include the following:

- ✓ Thermal stress
- ✓ Induction heating
- ✓ Induction stirring
- ✓ Steady-state fluid-structure interaction
- ✓ Magneto-structural interaction
- ✓ Electrostatic-structural interaction
- ✓ Current conduction-magnetostatics

The ANSYS program can perform multiphysics analyses with a single ANSYS database. A single set of nodes and elements will exist for the entire model. What these elements represent are changes from one physics analysis to another, based on the use of the physics environment concept.

There are basically two methods of coupling distinguished by the finite element formulation techniques used to develop the matrix equations: Strong (also matrix, simultaneous, or full) coupling, and Weak (also load vector or sequential) coupling. These are illustrated here with two types of degrees of freedom ({X1}, {X2}):

In strong coupling the matrix equation is of the form:

$$\begin{bmatrix} [k_{11}] & [k_{12}] \\ [k_{21}] & [k_{22}] \end{bmatrix} \begin{Bmatrix} \{x_1\} \\ \{x_2\} \end{Bmatrix} = \begin{Bmatrix} \{F_1\} \\ \{F_2\} \end{Bmatrix} \quad \text{.....4.1}$$

and the coupled effect is accounted for by the presence of the off-diagonal submatrices $[K_{12}]$ and $[K_{21}]$. This method provides for a coupled response in the solution after one iteration.

In weak (also load vector or sequential) coupling, the coupling in the matrix equation is shown in the most general form:

$$\begin{bmatrix} [k_{11}(\{x_1\},\{x_2\})] & 0 \\ 0 & [k_{22}(\{x_1\},\{x_2\})] \end{bmatrix} \begin{Bmatrix} \{x_1\} \\ \{x_2\} \end{Bmatrix} = \begin{Bmatrix} \{F_1(\{x_1\},\{x_2\})\} \\ \{F_2(\{x_1\},\{x_2\})\} \end{Bmatrix} \quad \text{.....4.2}$$

and the coupled effect is accounted for in the dependency of $[K_{11}]$ and $\{F_1\}$ on $\{X_2\}$ as well as $[K_{22}]$ and $\{F_2\}$ on $\{X_1\}$. At least two iterations are required to achieve a coupled response. Note that both method of couplings are used in thermal structural analysis, unlike others coupled fields.

4.3.2 General Analysis Procedures

You can perform a sequential coupled-field analysis using either separate databases or a single database with multiple physics environments.

In the separate databases, you maintain different databases and results files. Figure 4.8 shows the data flow for a typical sequential analysis done with the indirect method. Each data base contains the appropriate solid model, elements, loads, etc. You can read information from a results file into another database. Element and node numbers must be consistent between the databases and the results file.

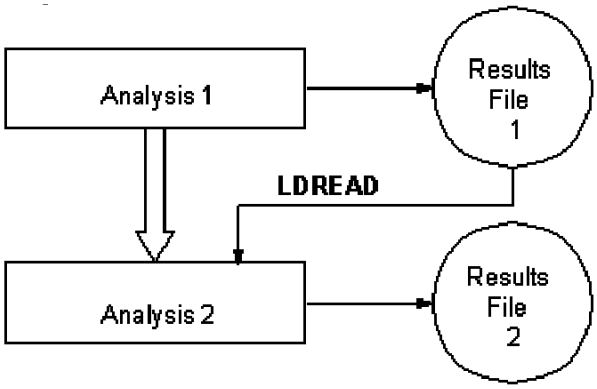

Figure 4.9 data flow for a typical sequential analysis done with the indirect method

The basic procedure in this problem is as follows:

- ✓ Define and solve the thermal problem.
- ✓ Return to PREP7 and modify the database. You will need to switch element types, specify additional material properties, and specify structural boundary conditions.
- ✓ Read the temperatures from the thermal results file.
- ✓ Solve the structural problem

In multiple physics environments approach, a single database exists for the entire model. Figure 4.9 shows the data flow using the multiple physics environment approach. The database must

contain the elements and nodes for all the physics analyses which you undertake. For each element or solid model entity, you must define a set of attribute numbers. These include an element type number, a material number, a real constant number, and an element coordinate system number. All of these numbers will remain constant across all the analyses. However, the actual properties associated with a given attribute number can vary among all the physics environments, as can the definition of the parameters in real constant sets and the element type number [31].

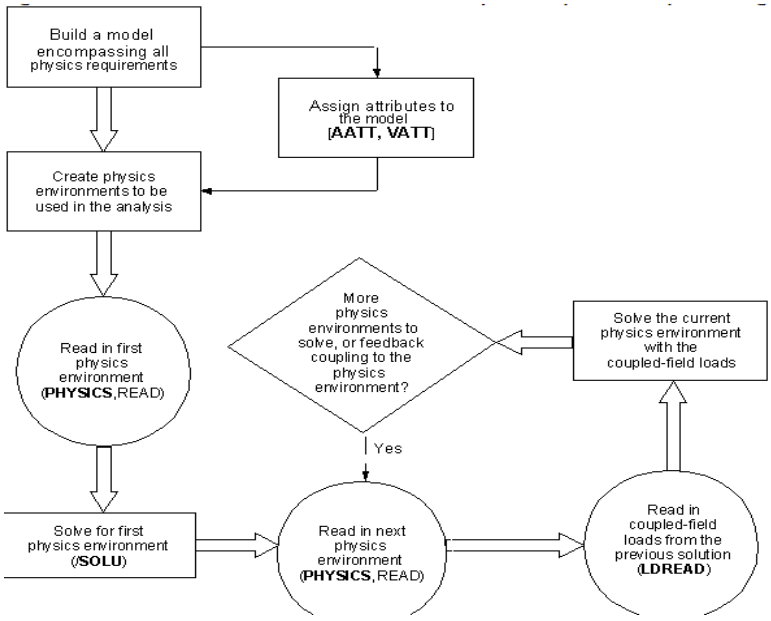

Figure 4.10 Data flow using the multiple physics environment approach.

The basic procedures for the physics environment approach shown below:

1. Define the thermal problem.

2. Write the thermal physics file.

3. Clear boundary conditions and options.

4. Define the structural problem.

5. Write the structural physics file.

6. Read the thermal physics file.

7. Solve and postprocess the thermal problem.

8. Read the structural physics file.

9. Read the temperatures from the thermal results file.

10. Solve and postprocess the physics file

Multiple Physics Environments shows you how to solve the same thermal-stress problem covered in Separate Databases, this time using the physics environment approach. In this particular case, it may not be advantageous to use the physics environment approach because the problem is a simple one-way coupling. However, it will allow for quick switching between physics environments for subsequent modeling or analysis.

The solution sequence follows the standard finite element methodology. Convergence is achieved when changes in all unknowns. There are different kinds of coupled-field analyses including methods of coupling present in each analysis, such as Thermal-Structural Analysis, Magneto-Structural Analysis (Vector Potential), and Electro-Thermo-Structural Analysis which have different application areas. Some of the coupling described above is always or usually one-way. For example, Thermal-Structural coupling, the temperatures affect the displacements of the structure by way of the thermal strains, but the displacements usually do not affect the temperatures. This thesis focuses on Thermal-Structural coupling.

4.3.3 Thermal-Structural Analysis

To investigate the thermal stress behavior of brake discs under cyclic thermal load, it is necessary to obtain typical temperature distributions in these brake discs as a function of time. Therefore, the objective of this section is to predict the temperature response of the disc. The material properties required for the temperature analysis in brake discs include the density, specific heat capacity and thermal conductivity. Table 3.3 shows the grade 150 cast iron used. To determine the temperature distribution, the physical conditions existing at the boundaries must be defined such as surface heat fluxes and convective heat transfer coefficients at free surfaces.

The same brake rotor model was analyzed for thermal stress at each time step of the thermal analysis for both finite element method and analytical method. The predicted non-uniform

temperature distributions from the thermal analysis were used as the input data in this analysis. To evaluate the thermal stresses caused by these temperature distributions, stress components (axial, radial and circumferential stresses) and the elastic von Mises stress was considered, since these parameter, which combines the three principal stresses. These parameters are assumed to determine yield (onset of plastic deformation) in metals. Elastic stresses and strains are completely reversible and non cumulative in disc brake [4], therefore the brake disc model was investigated for only one cycle of the braking period.

The descriptions Thermal-Structural coupling phenomena includes applicable analysis types, applicable element types, and basic matrix equations, including the matrix and/or vector terms possible in each analysis type.

Element types: SOLID186, PLANE13, SOLID98, PLANE223, SOLID226, SOLID227

Matrix equation:

(b) Strong coupling

$$\begin{bmatrix}[M] & [0]\\ [0] & [0]\end{bmatrix}\begin{Bmatrix}\{\ddot{u}\}\\ \{\ddot{T}\}\end{Bmatrix}+\begin{bmatrix}[C] & [0]\\ [C^{tu}] & [C^{t}]\end{bmatrix}\begin{Bmatrix}\{\dot{u}\}\\ \{\dot{T}\}\end{Bmatrix}+\begin{bmatrix}[k] & [0]\\ [k^{tu}] & [k^{t}]\end{bmatrix}\begin{Bmatrix}\{u\}\\ \{T\}\end{Bmatrix}=\begin{Bmatrix}\{F\}\\ \{Q\}\end{Bmatrix} \quad \text{.....4.3}$$

(b) Weak coupling

$$\begin{bmatrix}[M] & [0]\\ [0] & [0]\end{bmatrix}\begin{Bmatrix}\{\ddot{u}\}\\ \{\ddot{T}\}\end{Bmatrix}+\begin{bmatrix}[C] & [0]\\ [0] & [C^{t}]\end{bmatrix}\begin{Bmatrix}\{\dot{u}\}\\ \{\dot{T}\}\end{Bmatrix}+\begin{bmatrix}[k] & [0]\\ [0] & [k^{t}]\end{bmatrix}\begin{Bmatrix}\{u\}\\ \{T\}\end{Bmatrix}=\begin{Bmatrix}\{F\}+\{F^{th}\}\\ \{Q\}+\{Q^{ted}\}\end{Bmatrix} \quad \text{.....4.4}$$

Where: $[k^{t}]=[k^{tb}]+[k^{tc}]$

$$\{F\}=\{F^{nd}\}+\{F^{pr}\}+\{F^{ac}\}$$

$$\{Q\}=\{Q^{nd}\}+\{Q^{g}\}+\{Q^{c}\}$$

$\{u\}$ is displacement vector

$\{T\}$ is thermal potential (temperature) vector

$\{\dot{T}\}$ is time derivative of thermal potential (temperature) vector

ü is time derivative of displacement

ü is second time derivative of displacement

[M] is structural mass matrix (Coefficient matrices of second time derivatives of unknowns.) (discussed in Derivation of Structural Matrices

[C] is structural damping matrix (Coefficient matrices of first time derivative of unknowns) (discussed in Derivation of Structural Matrices)

$[C^t]$ is thermal specific heat matrix (discussed in Derivation of Heat Flow Matrices)

$[C^{tu}]$ is thermoelastic damping matrix (discussed in Thermoelasticity)

[K] is structural stiffness matrix (Coefficient matrices of unknown) (discussed in Derivation of Structural Matrices)

$[K^t]$ is thermal conductivity matrix (may consist of 1, 2, or 3 of the following 3 matrices) (discussed in Derivation of Heat Flow Matrices)

$[K^{tb}]$ is thermal conductivity matrix of material (discussed in Derivation of Heat Flow Matrices)

$[K^{tc}]$ is thermal conductivity matrix of convection surface (discussed in Derivation of Heat Flow Matrices)

$[K^{ut}]$ is thermoelastic stiffness matrix (discussed in Thermoelasticity)

$\{F^{nd}\}$ is applied nodal force vector (discussed in Derivation of Structural Matrices)

$\{F^{pr}\}$ is pressure load vector (discussed in Derivation of Structural Matrices)

$\{F^{ac}\}$ is force vector due to acceleration effects (i.e., gravity) (discussed in Derivation of Structural Matrices)

$\{F^{th}\}$ is thermal strain force vector (discussed in Derivation of Structural Matrices)

$Q^{nd}\}$ is applied nodal heat flow rate vector (discussed in Derivation of Heat Flow Matrices)

$\{Q^c\}$ is convection surface vector (discussed in Derivation of Heat Flow Matrices)

$\{Q^g\}$ is heat generation rate vector for causes other than Joule heating (discussed in Derivation of Heat Flow Matrices)

$\{Q^{ted}\}$ is heat generation rate vector for thermoelastic damping

4.3.4 Element used in thermal analysis

SOLID90 is used for thermal analysis of the rotor [31]. SOLID90 is a higher order version of the 3-D eight node thermal element (SOLID70). The element has 20 nodes with a single degree of freedom, temperature, at each node. The 20-node elements have compatible temperature shapes and are well suited to model curved boundaries. The 20-node thermal element is applicable to a 3-D, steady-state or transient thermal analysis. If the model containing this element is also to be analyzed structurally, the element should be replaced by the equivalent structural element (such as SOLID186).

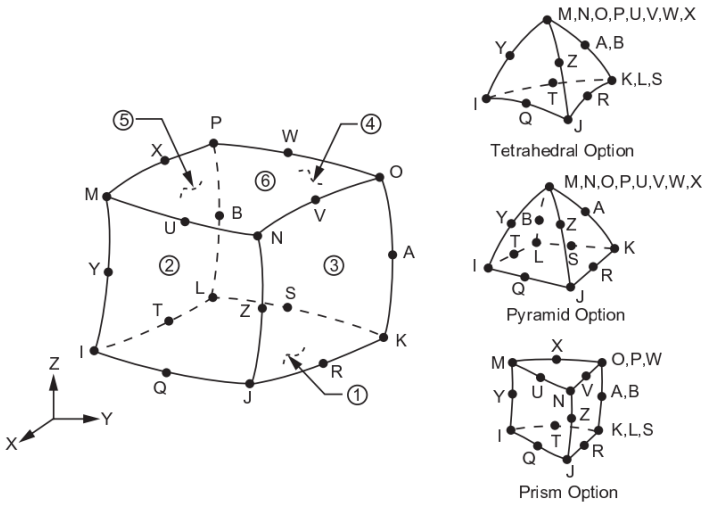

Figure 4.11 SOLID90 Geometry

The geometry, node locations, and the coordinate system for this element are shown in Figure 4.10. The element is defined by 20 node points and the material properties. A prism-shaped element may be formed by defining duplicate K, L, and S; A and B; and O, P, and W node numbers. A tetrahedral-shaped element and a pyramid-shaped element may also be formed as shown in Figure 4.10.

There is nodal loading condition in this element. Convection or heat flux (but not both) may be input as surface loads at the element faces as shown by the circled numbers on Figure 4.10. Heat generation rates may be input as element body loads at the nodes. If the node I heat generation rate HG (I) is input, and all others are unspecified, they default to HG (I). If all corner node heat generation rates are specified, each midside node heat generation rate defaults to the average heat generation rate of its adjacent corner nodes. The solution output associated with the element is in nodal temperatures included in the overall nodal solution.

4.3.5 Element Used in Stress Analysis

SOLID186 is a higher order 3-D 20-node solid element that exhibits quadratic displacement behavior. The element is defined by 20 nodes having three degrees of freedom per node: translations in the nodal x, y, and z directions. The element supports plasticity, hyperelasticity, creep, stress stiffening, large deflection, and large strain capabilities. It also has mixed formulation capability for simulating deformations of nearly incompressible elastoplastic materials, and fully incompressible hyperelastic materials. SOLID186 is available in two forms: Homogenous Structural Solid (KEYOPT(3) = 0, the default) and Layered Structural Solid (KEYOPT(3) = 1) [31].SOLID186 Homogenous Structural Solid is well suited to modeling irregular meshes. The element may have any spatial orientation.

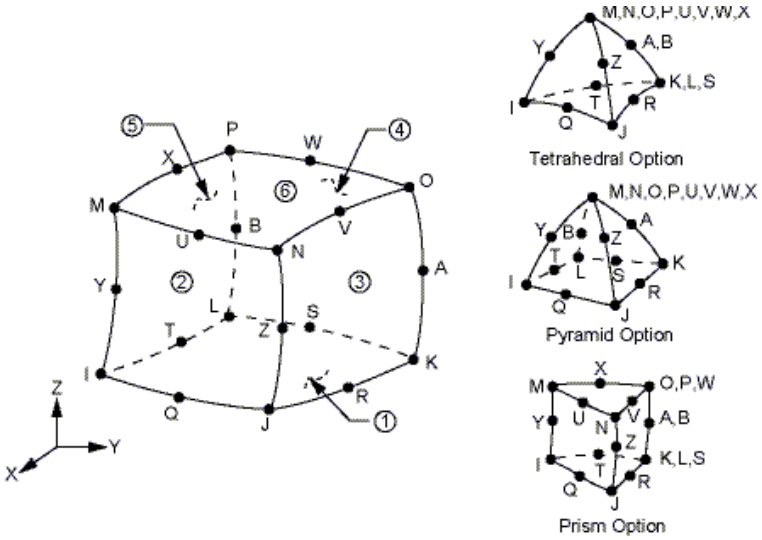

Figure 4.12 SOLID186 Homogenous Structural Solid Geometry

The geometry, node locations, and the element coordinate system for this element are shown in Figure 4.11. A prism-shaped element may be formed by defining the same node numbers for nodes K, L, and S; nodes A and B; and nodes O, P, and W. A tetrahedral-shaped element and a pyramid-shaped element may also be formed as shown in Figure 4.11. SOLID187 is a similar, but 10-node tetrahedron element. In addition to the nodes, the element input data includes the anisotropic material properties. Anisotropic material directions correspond to the element coordinate directions.

Element loads are described in nodal loading. Pressures may be input as surface loads on the element faces as shown by the circled numbers on Figure 4.11. Positive pressures act into the element. Temperatures may be input as element body loads at the nodes. The node I temperature T(I) defaults to TUNIF (uniform temperature). If all other temperatures are unspecified, they default to T(I). If all corner node temperatures are specified, each midside node temperature defaults to the average temperature of its adjacent corner nodes. For any other input temperature pattern, unspecified temperatures default to TUNIF. SOLID186 homogenous structural solid input summary is listed below.

Nodes

I, J, K, L, M, N, O, P, Q, R, S, T, U, V, W, X, Y, Z, A, B

Degrees of Freedom: - UX, UY, UZ

Real Constants: - None

Material Properties: - EX, EY, EZ, ALPX, ALPY, ALPZ, PRXY, PRYZ, PRXZ (or NUXY, NUYZ, NUXZ), DENS, GXY, GYZ, GXZ, ALPD, BETD

Surface Loads: - Pressures

face 1 (J-I-L-K), face 2 (I-J-N-M), face 3 (J-K-O-N),

face 4 (K-L-P-O), face 5 (L-I-M-P), face 6 (M-N-O-P)

Chapter Five: Results and Discussion

In this section, results of finite element approach for temperature and thermal stress estimation in ANSYS and analytical method is compared. The result of the analysis summarized as follow. Temperature distribution of analytical analysis is almost the same to that of ANSYS. But, thermal stress of analytical analysis is somewhat greater than ANSYS both in compressive as well as tensile stresses. Analytical and ANSYS temperature distribution is compared to check whether the similarity of the input for thermal stress analysis in ANSYS and analytical analyses is maintained. Unless the thermal analysis is approached, we cannot compare thermal stresses.

5.1 Temperature distribution through the thickness of the disc.

Figures 5.1 show temperature contour plots predicted by the FE analysis at the end of the first brake application. In order to investigate the temperature and von Mises stress histories, surface and thickness of the disc is selected, because surface areas are subjected to high temperatures and stresses and these parameters are reduced through the thickness according to the contour plot result, as well as the graph of figure 5.2

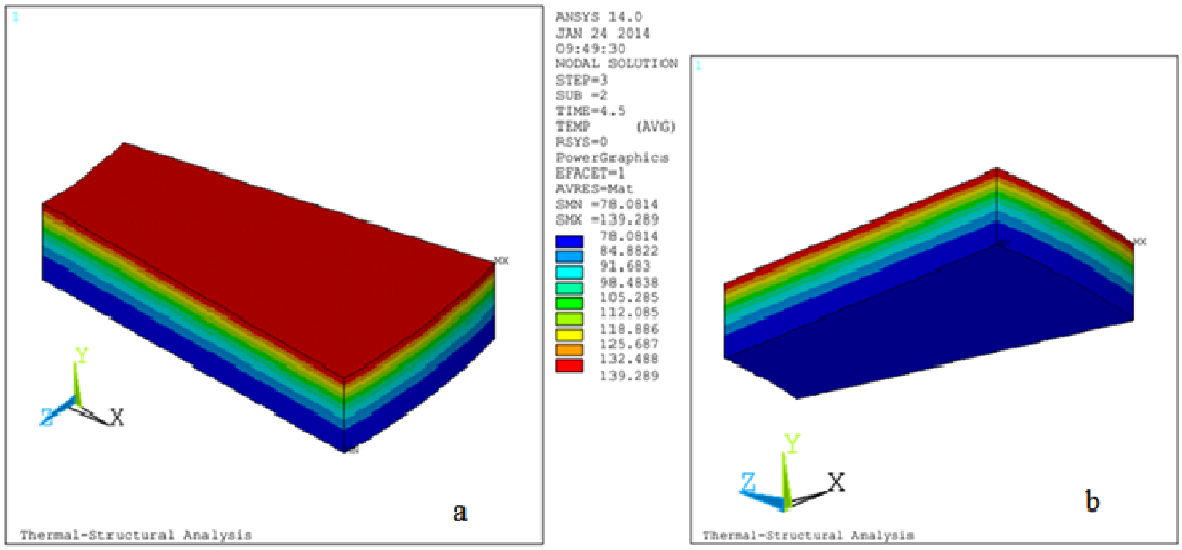

Figure 5.1Contour plot of temperature through disc thickness with different orientation (a and b)

From figure 5.1, the temperature gradient between the rubbing surface and far from the surface is large at the end of the brake application, which may result in high thermal stresses at the

surface. The difference in temperature between the rubbing surface and lower part, as shown from figure 5.2 is 61.119^{o}C by ANSYS (139.2 ^{o}C -78.081 ^{o}C) and 65.654 ^{o}C analytically (144.2778 ^{o}C -78.6238 ^{o}C) after 4.5 seconds.

As described in section 4.3.3, the coupled field analysis consist of two analysis type: therma1 (transient) and structural (static). Transient thermal analyses determine temperatures and other thermal quantities that vary over time. Figure 5.2 shows thermal analysis through thickness at the end of brake application (4.5 sec.). A static structural analysis determines the displacements, stresses, strains, and forces in structures or components caused by loads that do not induce significant inertia and damping effects (dynamic effect). The analysis supports two types of thermal analysis: steady-state thermal analysis (temperature varying over a period of time can be ignored .i.e. Figure 5.2) and transient thermal analysis (temperature distribution under conditions that vary over a period of time .i.e. Figure 5.3)

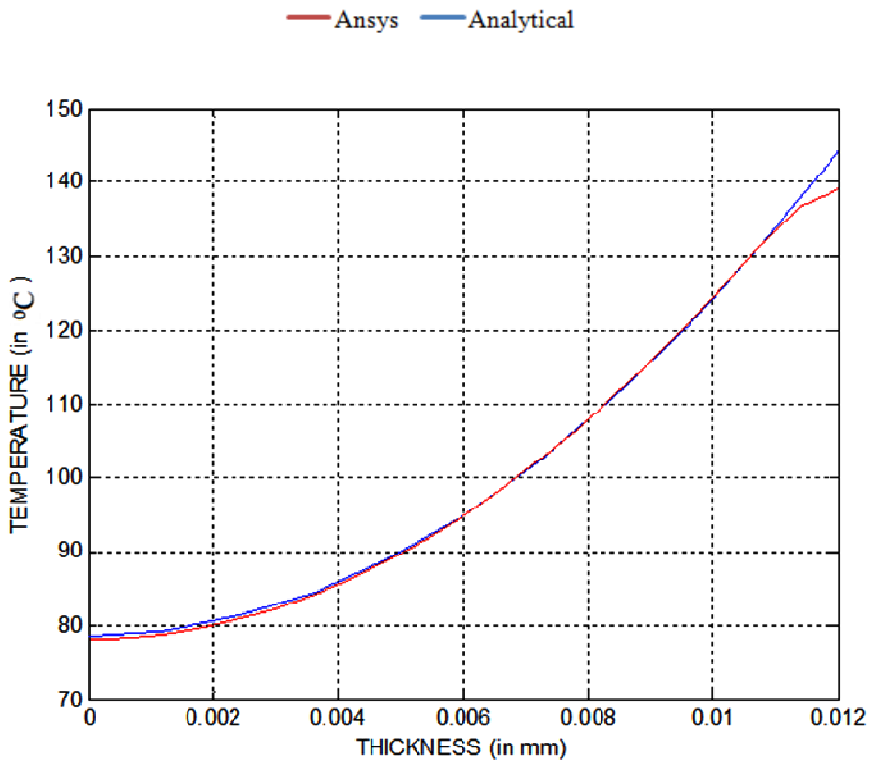

Figure 5.2 Steady state temperature distributions through the thickness at 4.5 seconds.

Using analytical analysis of dimensionless parameter we will have the same result along thickness of the disc, except on surface of the disc by using equation 3.37d. ANSYS estimates 5 ^{o}C less than analytical at the surface. The error percent between ANSYS and analytical is only 3% at the surface of the disc. This results the same input of temperature for analytical and ANSYS, and we expect related thermal stress.

The surface of the disc is highly exposed to the temperature over a braking time. As time of braking increase, the surface temperature increase to 144^{o}C. This reveals surface of the disc is a place where high thermal stress is expected. The same result is displayed analytically by equation 3.37d.The graph of analytical analysis and ANSYS is exactly the same as shown below.

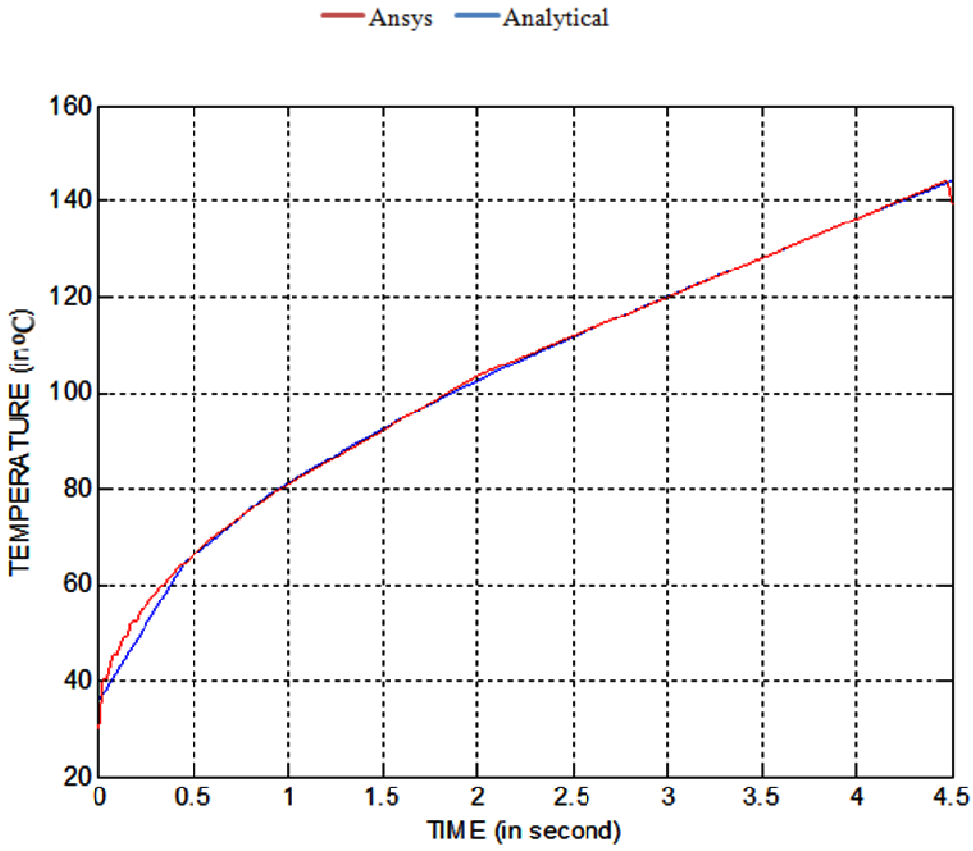

Figure 5.3 Transient surface temperature distributions

5.2 Circumferential stress through thickness of the disc

The same brake rotor finite element model as shown in Figure 5.1 for brake disc was analyzed for thermal stress at each time step of the thermal analysis. The predicted non-uniform temperature distributions from the thermal analysis were used as the input data in this analysis. To evaluate the thermal stresses caused by these temperature distributions, circumferential, radial, as well as the elastic von Mises stress defined in equation 3.43 was considered.

This is stress distribution perpendicular to the thickness of the disc. ANSYS result is displayed both by contour plot (figure 5.4) and graphically (figure 5.4). By ANSYS as well as analytically the minimum circumferential stress is found at far from the surface of the disc, where minimum temperature is expected, which is -122Mpa by ANSYS and -165Mpa analytically (equation 3.39b). The maximum circumferential compressive stress by ANSYS is found to be -276Mpa, and that of analytical is -388Mpa. ANSYS and analytical stress values at lower surface of the rotor are more related values than surface close to the pads. As we go through thickness of the disc from the bottom to surface of the disc, the variation of ANSYS and analytical analysis increases. This variation or non-correlated results are high near the contact surface; this might be due to relatively coarse mesh size, high symmetry dimension and large time steps used in transient analysis.

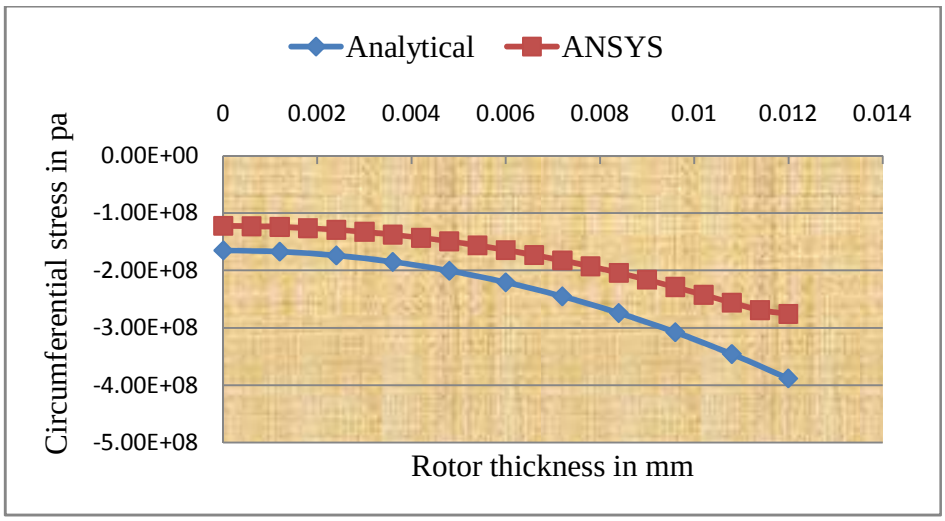

Figure 5.4 Compressive circumferential stresses as a function of disc thickness

The maximum and minimum stress obtained by ANSYS contour plot (Figure 5.5) is -590Mpa and -70.2Mpa respectively which are not only due to thermal stress, but stress concentration found at the sharp edge of the disc cut due to symmetry, and these values are not accepted as thermal stress values. If we remove symmetry these stresses are removed with symmetry. To get contour plot stress value similar to figure 5.4, stress is taken from thickness far from sharp edges, about 7.5° from both edges. At lower surface of the rotor contour plot, compressive stress is 128 Mpa which is related to figure 5.4. At surface of the rotor compressive stress ranges from -243 Mpa to 301 Mpa (figure 5.5a), an average value of 272Mpa which is same to ANSYS values of figure 5.4.

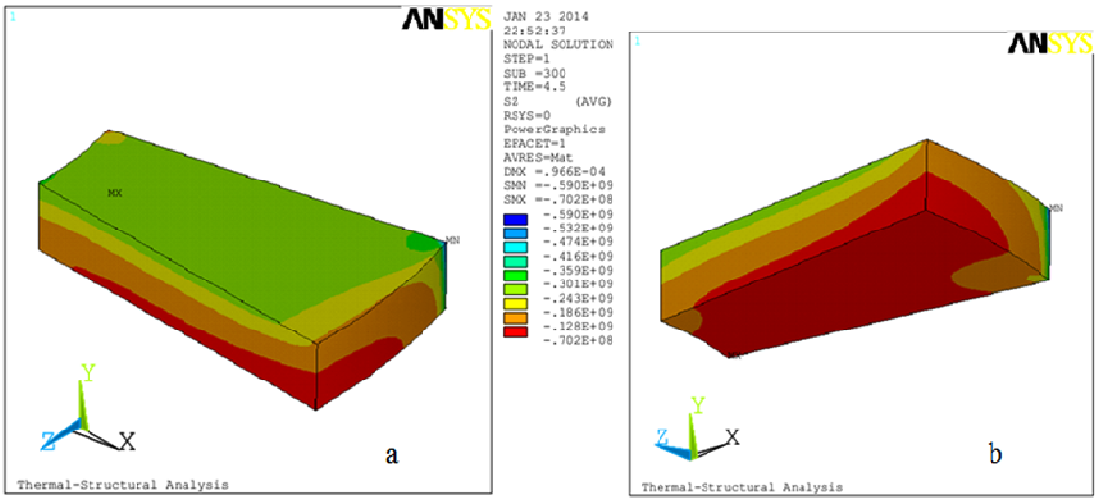

Figure 5.5 Contour plot of circumferential stress a) upper b) lower surface.

As it is seen in this section, when modeling any type of physical problem using finite element analysis, one has to understand the theory behind the phenomenon being modeled. Otherwise, the results obtained (in this case stress at edges of contour plot) could be misleading and potentially dangerous if blindly relied upon. The contour plot as well as the graph of figure 5.4 shows that the stress produced is compressive stress only. This is due to the fact that the thickness of the rotor is sandwiched between the two pads during braking. This stress is decreased as thickness increase from the surface.

5.3 Radial stress through thickness of the disc

The external radius of the disc is the only surface free from external constraint, which is free to expand radially. We can see from contour plot of figure 5.7 as well as from graph of figure 5.6 there is compressive as well as tensile radial stress, unlike that of circumferential stress which is compressive only. Both analysis shows that the thickness of the disc from 0 to 6.6mm is in tensile stress, and from 7mm to 12mm there is a compressive stress. ANSYS displays at lower surface of the rotor maximum tensile stress of 58.8Mpa as shown in figure 5.6. Analytically by equation 3.41b, 74.2Mpa is seen from figure 5.6 at the same position to that of ANSYS. This variation is reduced as we close to the mid thickness of the rotor. At thickness of 7mm both ANSYS and analytical have more related value than other positions.

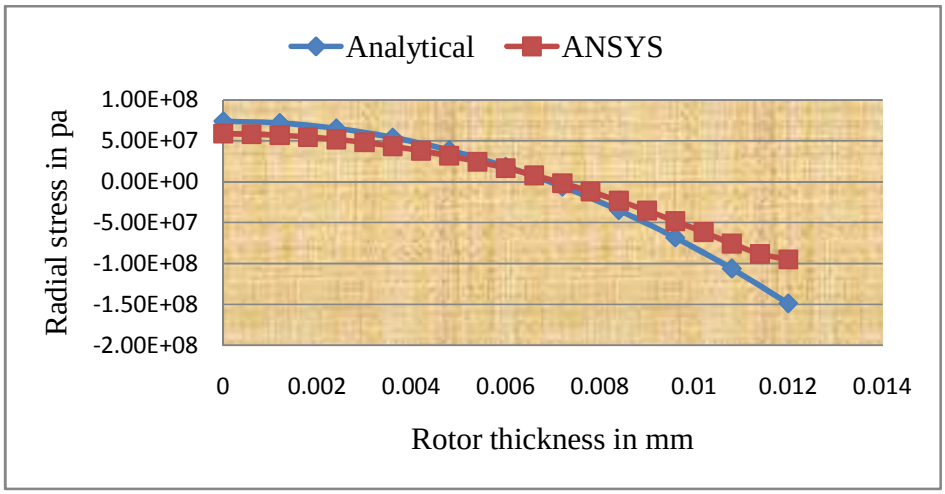

Figure 5.6 Radial stresses through thickness of the disc.

The graph of ANSYS and analytical cross one another at mid line of the thickness, because analytical analysis leads the ANSYS result both in tensile as well as in compressive. From this result we see that as the thickness approaches intersection line, ANSYS results coincide with analytical results. At surface of the disc there is large variation of ANSYS and analytical. This variation or non-correlated results are high near the contact surface; this might be due to relatively coarse mesh size and large time steps used in transient analysis and corrected by taking small piece of symmetry and increasing mesh refinement.

From contour plot (Figure 5.7) we can see that maximum tensile stress produced is 76.1 Mpa by ANSYS at the edge of lower surface, and analytically we will get 58.8Mpa at lower surface.

Again the maximum compressive stress from contour plot is -292Mpa which is found at edge of the upper surface. This value is greater than analytical analysis which is -150Mpa and cannot represents stress through thickness of the disc. As in the case of circumferential stress this stress is due to stress concentration at sharp edge in addition to thermal stress and cannot display correct stress distribution through thickness of the rotor.

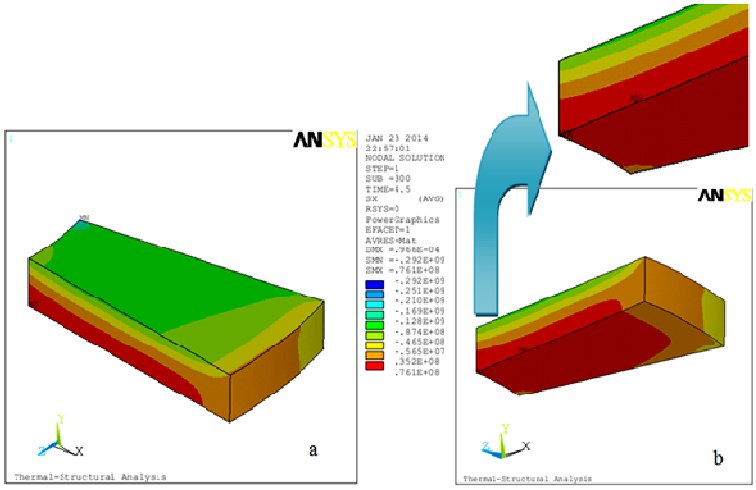

Figure 5.7 Contour plot of radial stress a) upper b) lower surface

When we take surface far from the edge where there is no influence of edge (about 7.5°), tensile stress ranges between 35.2Mpa and 76.1Mpa, which has average value of 55Mpa, related to ANSYS graph of figure 5.6 and decreases as the thickness closes to the surface. Compressive stress at the surface ranges between 87.4Mpa to128Mpa, which has average value of 107Mpa. Its average value approaches ANSYS value of Figure 5.6 which is -95Mpa at upper surface. The figure 5.6 shows this fact. Therefore we have to take path through thickness which if far from the edge (about 7.5 degrees) to fully describe stress through thickness.

5.4 Axial stress through thickness of the disc

Axial stress distribution is different from circumferential and radial, because temperature distribution is parallel to axial stress. Analytically it is predicted by equation 3.39c, which is -220Mpa and constant. But ANSYS predicts -175Mpa which varies negligible value through thickness of the disc. The figure below shows almost no variation of axial stress through thickness when we compare with other components of stress.

Figure 5.8 Variation of stress components through disc thickness

As it is seen from figure 5.8 axial stress is uniform with negligible variation through thickness of the rotor. The uniform distribution of axial stress is seen again from contour plot of figure 5.9 below. Axial stress of contour plot varies from compressive stress of 166Mpa to 189Mpa, with average value of 177Mpa.

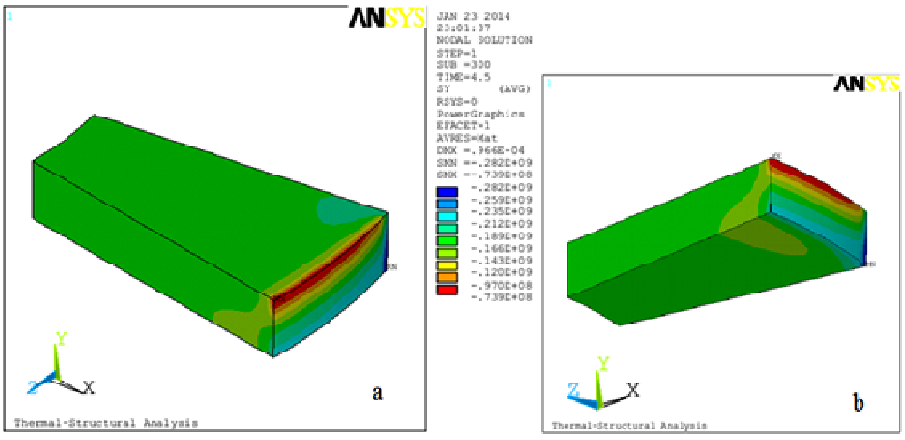

Figure 5.9 Variation of axial stress through disc thickness with different point of views a and b

From figure 5.8 we see that disc brake is highly exposed to compressive stress than tensile stress. Radial and circumferential stresses vary with thickness, with maximum value at the surface.

5.5 Von Mises Stress Through Thickness

Although analytical and ANSYS result of von Mises stress has the same geometry shape, analytical leads the ANSYS by of 26% accuracy at the surface of the disc. Figure 5.11 shows the accuracy increases as von mises approaches the surface.

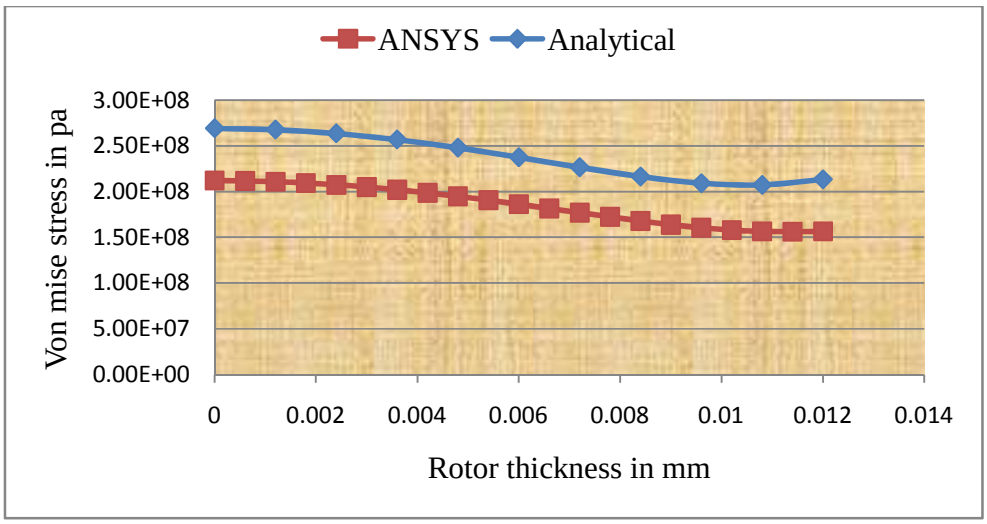

Figure 5.10 Von Mises stress through thickness

Maximum von Mises stress is found at surface far from pad contact, where high compressive stresses are found. Analytically by equation 3.43 maximum von Mises stress is 269Mpa and ANSYS predicts 212Mpa with 21% error. This error is minimized as we reduce the size of symmetry and increase mesh density.

The contour plot of figure 5.11 shows maximum von mises stress of 500Mpa and minimum von Mises stress of 67Mpa which are found at sharp edge created due to symmetry boundary condition. This high stress is caused due to stress concentration, in addition to thermally induced stress. But von Mises stress at surface far from edges (7.5°) is same to ANSYS result of figure 5.10. At lower surface, von Mises stress ranges from 211Mpa to 259Mpa, which is ANSYS value of figure 5.10. Minimum value of von Mises stress is found at surface which is 163Mpa from contour plot. There is 19% error between analytical and ANSYS. This error is reduced as we refine mesh size and time step of transient analysis.

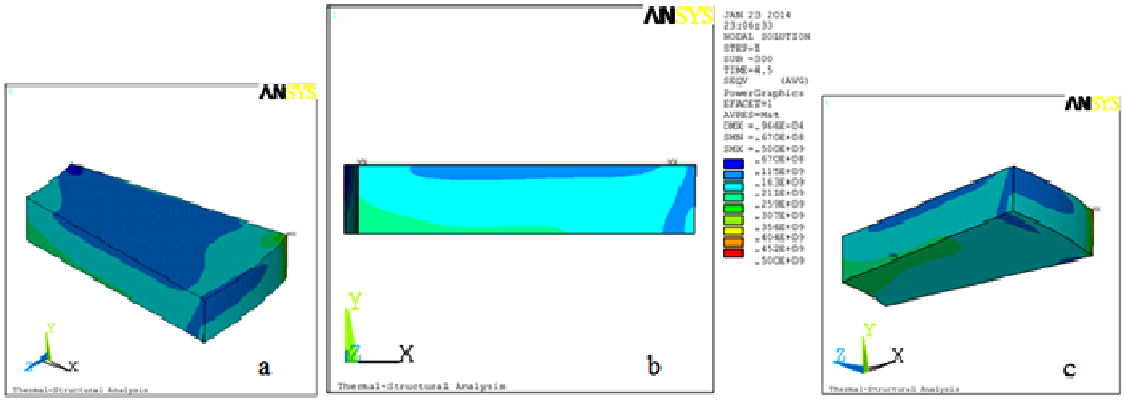

Figure 5.11 Contour plot of von Mises stress from different point of views (a, b, c)

Both analytical and ANSYS displays von Mises at the surface is lower than deep in the thickness, because there is radial tensile stress at the surface which cancels compressive forces.

It can be seen that the brake rotor has higher thermal stress on the surface far from rubbing surface (lower one) in comparison to the rubbing surface because the former is constrained from any thermal expansion due to symmetry, resulting in higher resistance to radial expansion. The rubbing surface is free to expand in any direction. Due to the bending resistance of the constrained surface, maximum von Mises stresses actually occur at the thickness far from rubbing surface (lower one).

5.6 Effect of Temperature on Brake Fade and coefficient of friction

Brake rotors are forced to absorb a significant amount of heat during braking. Brake fade describes a condition where heat is generated at a faster rate than they are capable of dissipating heat into the surrounding air. During this thermal analysis the temperature of rotor is increased up to 143 ^{o}C in just 4.5 seconds (figure 5.3). The typical generic "normal driving" temperature range for well balanced vehicle brakes is less than 135^{o}C. During repeated hard stops, overheating may occur and a loss of brake effectiveness or even failure may result. Primarily friction fade (lining fade) is caused by heat in disc brake. Friction fade affects disc brakes and occurs when the friction material overheats to the point where the coefficient of friction drops off. When the coefficient of friction drops off, friction is reduced and the brake assembly's ability to convert added heat is reduced.

5.7 Effect of Temperature on Tribo-layer Formation, Wear and Cracking

It is known that the pad/disc contact surfaces will change their characteristics due to friction, wear and other mechanical interaction at the interface as the friction braking distance increases. The interface temperature in the pad/disc contact (figure 5.3) is known to have a significant effect on friction. This can be explained from the fact that temperature affects the formation of so called tribolayers; surface active additives in the transmission surface that are present at the sliding interfaces in the pad/disc contact surfaces and which govern friction. The rate of generation of the tribolayer is influenced by the temperature dependant surface activity.

Materials are progressively removed from the surface due to thermomechanical stresses caused by the frictional interactions. As wear is high at the surface, the lower will be the operational life expectancy (figure 5.12). One explanation of this phenomenon is that as metal wear debris fills in the "open" area on the disc surface by mechanical means, the affinity between the two contact surfaces will increase. This makes the two contact surfaces more easily to form an adhesive bond (or welding junction). In order to withstand the friction motion a higher share force are required between disc and pad under the same normal load. Factors like sliding velocity, hydraulic pressure, time of braking, and their interactions are found to play a significant role in determining the wear rate.

Rotor cracking is a problem that particularly affects surface of disc subject to extreme thermal stress loading conditions at the surface (figure 5.8). Cracking arise from thermal energy input at the rubbing surfaces (figure 5.3) which became greater than the thermal energy output by convection. The temperature results obtained from analytical analyses, which assessed thermal partitioning between the pads and the rotor, were correlated with temperature measurements from FEM/ANSYS work. The result of the temperature analysis (figure 5.3) reveals that the occurrence of surface rupture and cracking in a single brake application depending on temperature induced (143 ^{o}C). During repeated braking, the Fatigue properties were a significant factor in determining the onset of rotor cracking.

5.8 Estimating Fatigue Life time of the Rotor

Plot of equivalent von Mises stress is shown in figure 5.10. It reveals that the mean equivalent stress of analytical analysis is roughly 241.31Mpa. Recall that the GG25cast iron alloy has yield

strength of 206Mpa (table 3.2). A close looks of figure 5.10 shows that the braking temperatures generate thermal stresses that clearly exceed the yield strength. This cycling between compression and tension, in phase with the temperature of the brake, is the thermomechanical responsible for failure.

The applied strain amplitude is estimated by calculating the elastic strain associated with the average equivalent rotor stress of 241.3Mpa (analytical of figure 5.10) giving $\varepsilon_{a=}$ 0.19% (from equation 3.46). The fatigue life time is found by plotting equation 3.47 over a broad range of strain amplitude ε_t using the fatigue constants for a GG25 grey cast iron alloy shown in table 3.5. As shown in figure 5.12 the fatigue life time associated with $\varepsilon_{a=}$ 0.19% is approximately 450 cycles to failure. Similarly by ANSYS, average equivalent rotor stress of 202Mpa is seen from figure 5.10, which gives strain amplitude of ε_a =0.155% (from equation 3.46). The fatigue life time associated with $\varepsilon_{a=}$ 0.155% is approximately 650 cycles to failure, even though SUV vehicle research and test center recommends more than this value.

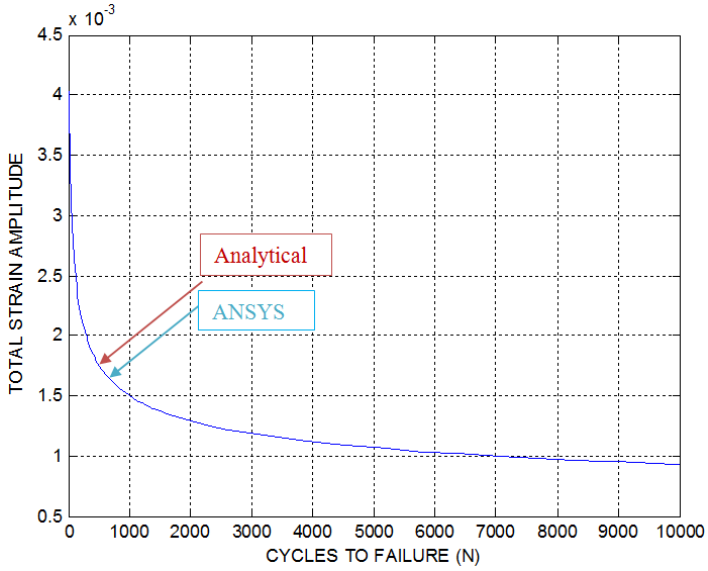

Figure 5. 12 Plot of Coffin-Manson law for GG25 gray cast iron alloy

Chapter Six: Conclusions and Recommendation

6.1 Conclusion

In this thesis work, FEA analysis procedure developed to study temperature and thermal stress in disc brake. The method developed in this thesis work can be used to analyze temperature and thermal stress in sliding contact mechanical components. Comparison of FEA result with analytical method is done and similar result is obtained with reasonable accuracy. Therefore, users may use FEA using ANSYS to estimate temperature and thermal stress developed in any mechanical components related to thermal stress. Generally from this thesis work the following conclusions can be figured out.

- ✓ Finite element analysis of temperature distribution exactly estimates temperature as a function of disc thickness and time. The result from FEA using ANSYS is agreeable with analytical with reasonable accuracy.
- ✓ Finite element analysis displays position of high and low stress distribution in similar manner with analytical analysis with tolerable accuracy of stress values. The path of maximum stress, and temperature, has similar shape through thickness.
- ✓ The contour plot display may not display stress through thickness exactly due to stress concentration at sharp edges. Instead of using contour plot of ANSYS, using path cross section through thickness of the disc gives similar result with analytical analysis.
- ✓ High circumferential stress variation occurs through the thickness when compared with axial stress which is almost constant.
- ✓ There is a combination of tensile and compressive radial stress through the thickness, with compressive at the surface, and tensile at surface far from the disc-pad contact point.
- ✓ There is a high temperature and stress components at the surface of the disc, and this may lead the surface to failure such as wear and rupture, because these parameters are a function of stress.
- ✓ This cycling between compression and tension, in phase with the temperature of the brake has direct influence on fatigue life of the brake rotor.
- ✓ Overheating of brake rotor leads loss of brake effectiveness in terms of surface rupture, crack initiation and fade of the brake.

6.2 Recommendation

From analytical analysis and Finite element analysis observations, it can be concluded that high temperature induced in disc/brake interface can results rotor fade, surface rupture and high stress, again which reduces life of the brake.

Different researchers specify different ways to eliminate thermal related problems in brake rotors. According to [32], increase in yield and fatigue strength of the rotor material, is one aspect. Even though the detail of increasing yield and fatigue strength was not given, it has direct influence on surface rupture, fade, and fracture of the rotor. In addition, decreasing brake temperature and redesigning the hub-rotor unit to eliminate constraint stresses were set as ways to improve brake performance in terms of life, failure and surface tribology.

The degree of increase of surface temperature depended on the thermal conductivity of the brake disc material. If the material had low thermal conductivity, the temperature gradient across the brake disc thickness was high. As a result, the surface temperature rose faster than that of the brake disc body, resulting in different thermal expansions between the surface and body of the brake disc. This problem is solved by gray cast iron material quality improvement: proportions of chemical compositions of the constituent. Increasing the carbon content in cast iron has the effect of increasing thermal conductivity. Fatigue life, as well as the behavior during cyclic loading, varies widely for different constituents of Carbon, Silicon, Manganese, and Sulfur and phosphorus.

Brake fade and rotor warping can be reduced through proper braking technique; when running down a long downgrade that would require braking simply select a lower gear (for automatic transmissions this may necessitate a brief application of the throttle after selecting the gear). Also, periodic, rather than continuous application of the brakes will allow them to cool between applications. Continuous light application of the brakes can be particularly destructive in both wear and adding heat to the brake system.

Another technique employed to prevent brake fade is the incorporation of fade stop brake coolers. Like titanium heat shields the brake coolers are designed to slide between the brake pad backing plate and the caliper piston. They are constructed from a high thermal conductivity, high yield strength metal composite which conducts the heat from the interface to a heat sink which is

external to the caliper and in the airflow. They have been shown to decrease caliper piston temperatures by over twenty percent and to also significantly decrease the time needed to cool down.

6.3 Future Work

In this thesis work temperature and thermal stress distribution along thickness of the disc is studied. Other influencing factors are not studied. So this work is restricted to the specified cases. However, this paper can be extended to other situation listed below. Further numerical method investigations should be conducted on:

- ✓ Fatigue analysis of disc brake under repeated brake application with time varying heat flux applied at the disc surface
- ✓ Fracture mechanics approach to study surface stress related to initiation and propagation of cracks by stress varying along radius of the disc.
- ✓ Hot spots analysis as a result of high local temperatures on the brake disc, hot spots may form and lead to undesirable performance hindrances such as brake fade or vibrations and judder.
- ✓ Vibration analysis caused by stress components
- ✓ Wear and noise analysis of disc brake caused by thermally induced surface stress

References

1. **Lanchester**: 'Velocity and relative contact size effect on the thermal constriction resistance in sliding solids'. ASME J. Heat Transfer, 119 (1997) 173-177.
2. **Dr. Z. Amps, Disc brake:** 'Facts, Discussion Forum, and Encyclopedia Article'. http://www.absoluteastronomy.com/topics/Disc_brake p 1 of 6. 11/19/13 11:30 AM.
3. **Medonos, S.:** 'Study of Structural Behavior of Ventilated Brake Disc'. SAE Technical Paper Series: 831316, 1983.
4. **S. Koetniyom:** 'Thermal Stress Analysis of Automotive Disc Brakes'. PhD Thesis, The University of Leeds School of Mechanical Engineering, 2010.
5. **T. Hogskolan:** 'Simulation of thermal stresses in a disc brake'. Product Development and Materials Engineering, MSc Thesis, School of Engineering in Jönköping, 2012.
6. **Samie, F. and Sheridan, D. C.:** 'Contact analysis for a passenger car disc brake', SAE Technical Paper Series: 900005, 1990.
7. **Lee, Y. S., Brooks, P. C., Barton, D. C. and Crolla, D. A.:** 'A Study of Disc Brake Squeal Propensity Using a Parametric Finite Element Model', Vehicle Noise and Vibration, IMechE Conference Transactions No C521/009/98,1998.
8. **Yano, M. and Murata, M.:** 'Heat flow on Disc brakes'. SAE Technical Paper Series: 931084, 1993.
9. **Limpert, R.:** 'The Thermal Performance of Automotive Disc Brakes', SAE Technical Paper Series: 750873, 1975.
10. **Noyes, R. N. and Vickers P. T.:** 'Prediction of Surface Temperatures in Passenger Car Disc Brakes', SAE Technical Paper Series: 690457, 1969.
11. **J. G. Balotin**. 'The influence of temperature on the friction coefficient of friction materials' ABCM Symposium Series in Mechatronics - Vol. 4 - pp.898-906
12. **T Nakatsuji, K Okubo, T Fujii, M Sasada, Y Noguchi (2002):** 'Study on Crack Initiation at Small Holes of One- piece Brake Discs'. Society of Automotive Engineers, Inc 2002-01-0926.
13. **G. Babukanth & M. Vimal Teja:** "Transient Analysis of Disk Brake By using Ansys Software", pp-23-24.
14. **M. Hamraoui:** 'Thermal behavior of rollers during the rolling processes'. Applied Thermal Engineering, 29 (11-12) (2009) 2386-2390.
15. **M. Hamraoui, Z Zouaoui:** 'Modelling of heat transfer between two rollers in dry friction'.

16. **J. B. hairier:** ‘Themie Analyaque de la Chaleur’. Paris, 1822 (English .trans. by A. Freeman, Dover Publications, Ncw York, 1955).
17. **A. Belhocine** and **M. Bouchetara:** ‘Simulation of fully coupled thermomechanical analysis of disc brake rotor’. University of of Oran WSEAS transactions on applied and theoretical mechanicsIssue 3, Volume 7, July 2012
18. **Jacobsson:** ‘Aspects of Disc Brake Judder’. Professional Engineering Publishing, Volume 217. Number 6. pp. 419-430, 2003.
19. API 579 Fitness-for-Service-API Recommended Practices 579, First Edition, January 2000, American Petroleum Institute.
20. **Chandrasekharaiah DS, and Debnath L:** ‘Continuum Mechanics’. Academic Press, Boston, 1994.
21. **B.A. Boley, J. Weiner:** ‘Theory of Thermal Stresses’. John Wiley & Sons, 1960.
22. **Evtushenko, O. O., Ivanyk, E. H., Horbachova, N. V.:** ‘Analytic methods for thermal calculation of brakes (review)’. Materials Science, Vol. 36, pp. 857–862, 2000.
23. **Bansal and Streater:** ‘Heat conduction in disk brake’, 2008.
24. **David V. Hutton:** ‘Fundamentals of finite element analyses’. p-228, New York: McGraw-Hill, 2004.
25 **Majcherczak D, Dufrenoy P (2007):** ‘Tribological, thermal and mechanical coupling aspects of the dry sliding contact’. Tribol Int 40:834–843. doi: 10.1016/j.triboint.2006.08.004.
26 **D. W. Mackowski:** ‘Conduction Heat Transfer’. Auburn University, Mechanical Engineering Department, 2010, P 72.
27 **S. Timoshenko and J. N. Goodier:** ‘Theory of Elasticity’. P-399: New York: McGraw-Hill, 1951.
28 **Fukano, A. and Matsui, H.:** ‘Development of Disc-Brake Design Method Using Computer Simulation of Heat Phenomena’. SAE Technical Paper Series 860634, 1986.
29 **Johnson, R. C.:** ‘Predicting Part Failures,’ Mach. Des., vol. 37, no. 1, pp 137-142,January 1965; no.2, pp. 157-162, January 1965.
30 MSC. Software, Reference Manual MD Nastran, Version r2.1, 2008.
31 ANSYS v.14 user’ Manual guide
32 Thomas J. Mackin. Thermal cracking in disc brakes. Engineering Failure Analysis 9 (2002) 63-76

Appendix I: Specification of SUV Car

Specification	SUV
Performance	- Min. steering diameter (m)-------- 12 - Max. speed km/hr ---------- 130 - Fuel tank capacity (L) ---------- 90 - AC capacity (kpa) ----------0.55 - Braking distance (km/hr) ---------- 25/60 - Parking brake grade angle (min) -----20^0 5min. not move - Idling speed (rpm) ---------- 800 - Emission ---------- Euro III -ON roadspeed performance----------130 OFF road speed performance----------90
Dimension	- Over all (l x w x h) mm -------- 4620 x 180 x 1830 - Frame (L x W) mm ---------- 4470 x 1740 - Cabin (l x h x w) mm -------- - Wheel base (mm) ------2730 - Wheel track front/rear (mm) --------- 1480/1492 - Min ground clearance (mm) ---------- 220
Electrical system	- Type single line negative grounded - Generator ---------- 12v/100A - Battery ---------- 12V/90A - Starter ---------- 12V
Mass	- Curb weight of chassis (kg) ----------910 - Axle load distribution front (kg) ---------- 1150 - Axle load distribution rear (kg) ----------1360 - G.V.W (kg) ---------- 1860 - Complete vehicle weight (kg) ----------2510 - Max load capacity (kg) ---------- 2510
Engine	- Model ---------- R425DOHC - 4 cylinder in line, 4 stroke , turbo charger, water cooled, inter cooler, electric control, common rail diesel engine -1 cylinder with 4 valves - Displacement ----------2499cc -Max output power (kw/r/min) --------- 105/4000 - Max torque (Nm/r/min) ----------340/2000 - Min fuel conception (g/kwh) ---------- 210 - Fuel conception (L/km) ---------- off road (L/100km)90km/h 10L on road 120km/h 12L
Clutch	- Single disc, dry type, friction clutch
Gear Box	- Mechanism ---------- 5 gear, reverse gear

	- Manual operated ------ 4 WD and 2 WD - Gear ratio --- I:4.016;II:2.318;III:1.401;IV:1.000;V:0.778;R:3.549
Steering mechanism	- Model ------- ZDZ7 - Circulating ball power steering, hydraulic assisted
Rack	- Front over suspension ------- Dual cross member independent, torsion bar - Rear cover suspension ------- torsion bar,5 bar coil spring
Wheel	- Rim --------- Aluminum type,17 inch - Tire ----------235/75R Spare tire
Cab	- Type ---------- all metal closed with AC - Seats ---------- 5 seats - electronic type AC and DVD entertainment system with Bluetooth - Door ---------- has indicator light has remote control - Seat cloth ---- leather laminated - Remote control of rear view mirror - Motor operated window glass - Electrical control of side indicator light under rear view mirror
Frame	- Mitsubishi tech.
Wheel Alignment	- Camber angle --------- 10'-1^0 10' - Caster angle ---------- 2^0 - 4^0 * The gap should be in – out (3 – 5) (mm)
Others	- Car model ---------- DD6470C - Color ---------- Silver/black - Safety energy absorbing steering column -Air bag
Breaking	- Parking brake ------- Handle cable, central control,Drum type - Front brake ------ Disc type - Rear brake ------ Disc type -Brake type--------ABS+EBD -Hydraulic pressure 1Mpa -81m stopping distance -Emergency braking time 4.5sec.
Over all weight	-Only vehicle (kg)-----1860 -Vehicle and load and also passenger + deriver (2510)